BAZ2A-SUV39H1-SMAD2/3-OCT4 regulates stemness, cell cycle exit and chemoresistance in pancreatic ductal adenocarcinoma

Stefania Militi
University of Oxford
Feng Liu
University of Oxford
Reshma Nibhani
University of Oxford
Mai Abdel Mouti
University of Oxford
Martin Pook
University of Oxford
Liuyang Cai
Southern University of Science and Technology
Siew Woh Choo
Wenzhou-Kean University
Siim Pauklin (siim.pauklin@ndorms.ox.ac.uk)
University of Oxford

Research Article

Keywords: Cancer stem cells, Pancreatic cancer, Epigenetics, TGFβ/ACTIVIN-SMAD2/3, Cell cycle, Cancer therapy

Posted Date: November 14th, 2023

DOI: https://doi.org/10.21203/rs.3.rs-3570401/v1

Additional Declarations: No competing interests reported.

Abstract

Tumorigenesis leads to the dedifferentiation of some cancer cells partly resemble stem cells. The maintenance circuitries and epigenetic regulatory complexes that regulate this stem cell-like state known as cancer stem cells (CSCs) are largely unclear. Here we aimed to find strategies for eliminating CSCs in pancreatic cancer (PDAC), one of the most metastatic and lethal cancers in human. Proteomic analyses of SMAD2/3 cofactors and screening of CSC self-renewal regulators uncovered BAZ2A and SUV39H1 as therapeutic targets of CSCs that cooperate with TGFβ/ACTIVIN-SMAD2/3 signalling in gene expression regulation. We show that Cyclin Dependent Kinase Inhibitor (CDKI) loci p14/p16 and p15 are silenced in CSCs by SMAD2/3-BAZ2A-SUV39H1 complex, and inhibiting BAZ2A and SUV39H1 reactivates silenced p14/p16/p15 that helps eliminating CSCs. Furthermore, the TGFβ/ACTIVIN signalling maintains a bivalent poised chromatin and enhancer-promoter 3D looping on CDKI, EMT and ABCC loci through SMAD2/3-SNON-PRC2-TrxG cooperating with OCT4/SOX2/NANOG. Elevated TGFβ/ACTIVIN signalling forms a positive feedback with p21/p57 that promotes a quasi-mesenchymal state of CSCs with increased EMT and higher G0 phase habitance that elevates CSC chemoresistance. Collectively, our study uncovers mechanisms how cell cycle regulation is hijacked in CSCs for supporting cellular plasticity, and how to circumvent this mechanism with combined treatment for targeted therapies.

Introduction

Pancreatic cancers are among the most lethal malignancies in humans [1]. While they account for approximately 3% of all new cancer cases, the mortality caused by pancreatic cancer is projected to surpass that of other common cancer types such as breast and colorectal cancer in the next decades, due to its late diagnosis, incidence of risk factors including obesity and metabolic syndrome [2], and limited response to treatment [3]. Pancreatic ductal adenocarcinoma (PDAC) is the most common type of pancreatic cancer, making up about 90% of all exocrine tumours [4]. Both ductal and acinar cells have been suggested as potential sources of precancerous lesions and a dedifferentiation of the cells to a progenitor-like or stem cell-like state with increased cellular plasticity seems to be a frequent event during pancreatic tissue transformation [5–13]. The existence of developmentally plastic cancer cells has been discovered in the brain, breast, colon, oesophagus, liver, lung, ovarian, prostate, stomach and thyroid cancers, among others. This dedifferentiated cell population in PDAC and other tumours, referred to as cancer stem cells (CSCs), acquires a stem cell-like state partially resembling to naturally occurring stem cells [14–16], which allows them to give rise to the whole tumour with its entire cellular heterogeneity. It also supports metastases formation and resistance to current cancer therapeutics by facilitating the escape from genotoxic insults caused by therapies. Annihilating CSCs is therefore needed for effective PDAC therapeutics.

The heterogeneous cancer cells in PDACs, including CSCs, are impacted by various signalling pathways that crosstalk with transcription factors and epigenetic regulators. Among these pathways is the TGFβ/Activin/Nodal-SMAD2/3 developmental signalling pathway. It plays a key function in early

development by controlling the self-renewal of human pluripotent stem cells (hPSCs), Epithelial-to-mesenchymal transition (EMT) and pancreatic tissue homeostasis [21–23]. The TGFß/Activin/Nodal-SMAD2/3 pathway regulates epigenetic mechanisms, for instance by cooperating with the core pluripotency protein NANOG and epigenetic modifiers such as DPY30-COMPASS to control pluripotency and differentiation of human pluripotent stem cells [24]. Aside from the key role of TGFβ/Activin/Nodal-SMAD2/3 in and developmental processes, this signalling pathway is directly involved in the formation of PDAC [22] and is frequently deregulated in PDAC [25 26]. The function of the pathway in PDAC is particularly interesting, because it confers dedifferentiated stem cell-like features to CSCs in PDAC [15], although the underlying mechanisms are still largely unknown.

To what extent CSCs undergo dedifferentiation, and how broadly they reactivate some molecular circuitries that are characteristic of developmentally earlier cellular states, is also largely unclear [17, 18]. CSCs are thought to have specific epigenetic mechanisms [18] that regulate their self-renewal in concert with signalling pathways, and the formation of CSCs has been postulated to occur as a result of epigenetic events [19]. Pancreatic CSCs have been found to express some components of the pluripotent stem cell circuitry, as exemplified by the detection of core pluripotency factors including SOX2, OCT4 and NANOG in a subset of pancreatic cancer cells [19, 20] and TGFβ signalling along with epigenetic regulatory enzymes [21, 22]. Furthermore, pancreatic CSCs have simultaneously ES cell-specific BAF (esBAF), and non-canonical BAF (ncBAF) and neural progenitor BAF (npBAF) epigenetic regulatory complexes [22] that cooperate with TGFβ/Activin-SMAD2/3 in regulating pancreatic CSC self-renewal, chemoresistance and invasiveness. The fact that several BAF complexes are present in CSCs is interesting given that each BAF complex is generally associated with distinct stem cell types: esBAF functions in regulating the self-renewal and pluripotency of embryonic stem cells, whereas npBAF is important for neural progenitor/neural stem cells, and non-canonical BAF is linked to naïve pluripotent stem cells [46]. This could reflect the developmentally plastic state of pancreatic CSCs [23], and their capacity to reversibly differentiate and dedifferentiate by using BAF complexes. Hence, the dynamics of different SMAD2/3-BAF complexes could provide the necessary stem cell-like developmentally plastic or “metastable” capacity of CSCs, as revealed for MLL in pancreatic CSCs [21]. Collectively, these discoveries suggest that CSCs utilize certain components of the molecular circuitries and epigenetic mechanisms that are usually present in stem cells at early developmental stages.

Cell proliferation and cell cycle progression are central for tumour suppression and it is a hallmark mechanism that is often deregulated in aggressive cancers. Understanding the orchestration of cell cycle regulation in the developmentally plastic CSCs in tumours is exceptionally important, because it will open new opportunities for developing more efficient cancer therapeutics. The progression of cell cycle in mammalian cells is primarily controlled by Cyclins and Cyclin Dependent Kinases (CDKs), which affect key transcriptional regulators such as Retinoblastoma protein (pRb). The activity of the Cyclin D/CDK complexes and thus cell proliferation is constrained by Cyclin Dependent Kinase Inhibitors (CDKIs), which are subdivided into two families. The INK4 proteins (p16INK4a, p15INK4b, p18INK4c, and p19INK4d) bind

to CDK4 and CDK6, and inhibit their kinase activities by interfering with their association with Cyclin D proteins [24] while the Kip/Cip proteins (p21Cip1, p27Kip1 and p57Kip2) inhibit Cyclin E-CDK2 [24, 25]. Importantly, the Cyclin D-CDK4/6 complex can also bind to Kip/Cip CDKIs. However, this interaction enhances Cyclin D-CDK4/6 activity since proteins such as p27 appear to limit INK4 CDKIs' capacity to bind this complex [26–28]. Hence, a complex combination of INK4 and KIP/CIP protein regulations determine cell cycle progression. *CDKN2A* encodes two cell cycle inhibitors, $p16^{INK4a}$ and $p14^{ARF}$, and is a hallmark gene deregulated in PDACs. It is inactivated in > 50% of PDAC cases often through gene silencing through abnormal promoter methylation or through mutations and deletions, which occur in PanIN2 precursor lesions [29]. In the presence of oncogenic stimuli such as constitutively elevated KRAS activation, $p14^{ARF}$ blocks interaction of MDM2 with p53, thereby promoting intracellular accumulation of p53 which in turn induces cell cycle arrest and/or apoptosis. The p16 and p53-mediated cell cycle arrest is induced in response to aberrant activation of oncogenic signalling and acts as a major barrier to malignant transformation [30]. In PDAC, p16 and p53 constrain tumour progression [31], while *Ink4a/Arf* deficiency accelerates formation of a highly invasive and metastatic cancer [32], suggesting that inactivation of *p14/p16* enables to circumvent KRAS-triggered oncogene-induced senescence and facilitates PDAC progression. $p14^{ARF}$ acts also through a p53-independent and CtBP2-dependent pathway to inhibit invasiveness and metastasis of pancreatic cancer cells [33]. Lastly, *p14/p16* mutation has been found to be associated with poor effector T cell and B cell but enriched regulatory T cell infiltration although this immunomodulatory effect is still mechanistically unclear [34]. Therefore, although *p14/p16* is best known for its role in regulation of cell cycle, the loss of encoded proteins contributes also to other aspects of PDAC biology. Of note, p15 deletion, that often happens with p14/p16 deletion in PDACs, is also essential for pancreatic cancer development instead of being just a co-deletion due to juxtaposition to p14/p16 [35].

We hypothesised that epigenetic or transcriptional mechanisms main CSC properties and that disruption of these mechanisms can help to eliminate CSCs. A small molecule compound screening identified BAZ2A and SUVH39H1 as regulators of CSC behaviour and proteomic analyses indicated the cooperation of SMAD2/3 with these epigenetic regulators at the chromatin level. Our results indicate that BAZ2A and SUVH39H1 are attractive therapeutic targets for specifically eliminating CSCs in PDACs.

Results

Compound screening identifies BAZ2A and SUV39H1 as regulators of pancreatic CSCs.

In order to find candidate epigenetic regulatory enzymes that are involved in controlling CSCs, and hence, could be used as therapeutic targets, we performed a screening experiment with 146 biologically active small molecule compounds against a broad range of epigenetic enzymes (Fig. 1a-b; Supplementary Table 1). For this screen, we established an endogenously tagged FG OCT4-GFP PDAC cell line, and screened for the expression of OCT4, CD133 and SSEA4 stem cell markers, in parallel to cell growth and apoptosis assessments (Fig. 1c). OCT4 is a transcription factor associated with high mortality in PDAC

[36], while the expression of cell surface receptor CD133 marks cells' efficiency in metastasizing [37, 38] and the cell surface glycolipid carbohydrate stage-specific embryonic antigen-4 (SSEA4) is expressed on the PDAC cell subpopulation and a wide range of cancers as well as pluripotent stem cells [39].

We uncovered that two BAZ2A inhibitors (BAZ2-ICR and GSK2801) [40, 41] and a SUV39H1 inhibitor (Chaetocin) [42], led to the reduction of OCT4+/CD133+/SSEA4 + cells (Fig. 1c-f). SUV39H1 is a protein lysine methyltransferase that introduces di- and trimethylation at H3K9 and has important roles in the maintenance of heterochromatin and gene repression [43, 44]. BAZ2A (TIP5) is a component of the nucleolar remodeling complex (NoRC), which regulates the expression of noncoding RNAs and heterochromatin in particular at centromeres and telomeres [45, 46]. In addition, elevated expression levels of BAZ2A have been reported in prostate cancer and it predicts disease recurrence [47].

We investigated the effect of BAZ2A and SUV39H1 on CSC self-renewal by tumour sphere assays by using both chemical inhibition with small molecules and genetic knockdown. Since Chaetocin has besides SUV39H1 targeting also several off-targets [42], we included an additional SUV39H1-specific small molecule inhibitor (F5446) for further investigation of this enzyme's involvement [48, 49]. F5446 and Chaetocin treatment of CSCs indicated reduced sphere numbers and sizes, which suggested a negative impact on CSC self-renewal in three PDAC cell lines (Fig. 1g; Supplementary Fig. 1a) and in PDAC patient primary tumour CSCs isolated by MACS for CD45- and CD133 + expression (Fig. 1h; Supplementary Fig. 1b). BAZ2A inhibition with both GSK2801 and BAZ2-ICR also reduced CSCs self-renewal and sphere size in three PDAC cell lines (Fig. 1i; Supplementary Fig. 1c) and in PDAC patient primary CSCs isolated by MACS for CD45- and CD133 + expression (Fig. 1j; Supplementary Fig. 1d). The genetic knockdown of SUV39H1 and BAZ2A expression similarly reduced CSC sphere formation thus confirming the results from chemical inhibition (Fig. 1k-l; Supplementary Fig. 1e-f). In addition, chemical inhibition as well as genetic knockdown of these factors reduced PDAC cell proliferation capacity (Fig. 1m-n) that resulted in the lengthening of the G1 phase whereas cells in G0 remained low (Fig. 1o). On the other hand, both SUV39H1 and BAZ2A inhibition increased cell apoptosis (Fig. 1p). Combined with Gemcitabine treatment, SUV39H1 or BAZ2A inhibition efficiently eliminated PDAC cells (Supplementary Fig. 1g-h).

Since SUV39H1 and BAZ2A inhibition impacted the proliferation of PDAC CSCs by extending the cell cycle primarily in the G1 phase, we hypothesised that their inhibition leads to the upregulation of cell cycle inhibitors. Since G1 phase is regulated by CDKIs we investigated their expression upon in CSCs upon the treatment with SUV39H1 and BAZ2A inhibitors. To investigate this we treated CSCs from PDAC lines with non-deleted p14/p16 loci with Chaetocin / F5446 and BAZ2-ICR / GSK2801 and analysed CDKI expression. qPCR analyses of CDKIs in CSCs treated with SUV39H1 and BAZ2A inhibitors for 72h led to the induction of p14 and p16 and to a lesser extent p15, and modestly also p18 (Fig. 1q). Furthermore, SUV39H1 and BAZ2A knockdown had a similar impact on the expression of these CDKIs (Fig. 1r). Flow cytometry analyses verified the induction of CDKIs in CSCs at the protein level upon the chemical inhibition of SUV39H1 and BAZ2A (Fig. 1s-t).

Collectively, our compound screening identified BAZ2A and SUV39H1 as novel regulators of pancreatic CSCs the can lead to the annihilation of CSCs upon their inhibition (Fig. 1q).

Proteomic analyses identify BAZ2A and SUV39H1 as interaction partners of SMAD2/3 in CSCs.

TGFβ/Activin/Nodal-SMAD2/3 signalling has contrasting effects on cells depending on the cellular context. This signalling pathway has anti-tumorigenic functions in normal non-cancerous cells that involves inhibitory effects on cell cycle progression. On the other hand, TGFβ/Activin/Nodal-SMAD2/3 promotes the self-renewal of human pluripotent stem cells. Interestingly, TGFβ/Activin/Nodal-SMAD2/3 signalling can also have dual functions in PDAC since at early stages, it primarily exerts anti-tumorigenic effects whereas at later stages, it acquires a pro-tumorigenic function. Due to these contrasting effects on cell cycle depending on the cell type, we were interested in understanding the effects of TGFβ/Activin/Nodal-SMAD2/3 signalling in CSCs.

Therefore, in parallel to the compound screening experiments, we performed proteomic analyses of SMAD2/3 in CSC, since the Activin A/TGFβ-SMAD2/3 signalling pathway has a major role in regulating the characteristics of CSCs through transcriptional regulation. We hypothesised that SMAD2/3 cooperate with previously uncharacterised epigenetic regulators on chromatin to achieve these effects in CSCs. The PDAC CSCs have increased CD44, PROM1/CD133, SSEA4 and CXCR4 expression in CSC spheres and have their characterization has been described before [21, 22]. To gain insight to the protein complexes that could mediate the effects of SMAD2/3 in CSCs, we performed SMAD2/3 Co-IP from nuclear extracts followed by mass-spectrometry (Fig. 2a). These proteomic analyses uncovered several epigenetic regulatory proteins that possess the enzymatic activity for controlling histone modifications, nucleosome repositioning and DNA methylation. Among the SMAD2/3 interaction partners were subunits of TrxG complex (e.g., DPY30, SNW1, OGT), PRC2/HDAC complexes (e.g., SAP18, EZH1, EED, JARID2, SMARCA5), MECP2 complexes (e.g. MECP2, NCOR1, NCOR2, SETD2, SETDB2), and DNA methylation complex (e.g., DNMT1, MDB3, ATRX) (Fig. 2b-d). These protein complexes are likely to cooperate with each other in gene expression regulation since STRING analyses of the mass-spectrometry data indicates their interactions (Fig. 2c). Importantly, among the interacting factors of SMAD2/3 in CSCs we identified BAZ2A that is a part of the NORC complex, and SUV39H1 that is part of the eNOSC complex. In combination with our compound screening experiments, these novel SMAD2/3 cofactors, BAZ2A and SUV39H1, seem to have an important regulatory function in CSCs, which leads to the annihilation of CSCs upon their inhibition by impacting the cell cycle progression and self-renewal.

Past research has shown that TGFβ/Activin-SMAD2/3 signalling is crucial for regulating the self-renewal and pluripotency of hPSCs by SMAD2/3-mediated transcriptional regulation of stem cell loci [50]. Since TGFβ/Activin/Nodal-SMAD2/3 signalling, self-renewal and cell cycle progression are interconnected [51], we investigated the expression of CDKIs in CSCs and pancreatic CSC responsiveness to Activin A/TGFβ signalling. We cultured PDAC A13A cells from single-cells in a 3D suspension condition, which enriches for CSCs due to their anoikis resistance. Comparison of Activin A treatment versus pathway inhibition with SB431542 for 48 hours by RNA-seq indicated that Activin A stimulation of CSCs upregulates p21

and p57 expression, and SB431542 downregulates these CDKIs, whereas no change was observed for other CDKIs (Fig. 2e). These results in CSCs were confirmed by qPCR and flow cytometry (Fig. 2f-h). Q-PCR analyses indicated that most of the CDKIs (p14, p15, p16, p18 and p57) have low expression in CSCs since the Ct values were similar to values observed in hPSCs, while hPSC-differentiated endoderm cells had a strongly elevated expression of most CDKIs compared to both hPSCs and CSCs (Supplementary Fig. 2a). Since the transcriptional effects on CDKIs indicated the regulation of these genes by TGFβ/Activin signalling, we analysed SMAD2/3 ChIP-seq data. We found SMAD2/3 binding onto the regulatory regions in the proximity of p14/p16, p15, p18, p21, p27 and p57 loci in hPSCs. Importantly, SMAD2/3 bind to these same regions in CSCs by SMAD2/3 ChIP-qPCR (Fig. 2i-j). We cloned the promoter regions containing SMAD2/3 binding elements into a luciferase expression vector and co-transfected them with SMAD3 expressing OE plasmid into PDAC cells. These promoter-luciferase assays further indicated the existence of an ACTIVIN/TGFβ/NODAL signalling dependent and SMAD2/3-mediated induction of CDKIs through their promoter regions that is blocked by SB431542 (Supplementary Fig. 2b).

CDKI loci are marked by both activating H3K4me3 and repressing H3K27me3 histone modifications in hPSCs (Fig. 2j), thus representing bivalent marks that are usually associated with developmental loci that are induced during tissue specification [52]. To determine if our newly identified SMAD2/3-interacting epigenetic regulatory complexes are involved in controlling the chromatin state of CDKI loci in CSCs, we performed ChIP-qPCR of the functional subunits of these complexes at SMAD2/3 binding sites. Interestingly, SUV39H1 and BAZ2A were enriched on p14/p16 and p15 loci, which was Activin A/TGFβ-SMAD2/3 signalling dependent, whereas the binding of SNW1 and DPY30 was absent on these loci in CSCs (Fig. 2k). In addition, SAP18, EZH1, and EED showed enrichment on p14/p16 and p15 loci, which was Activin A/TGFβ-SMAD2/3 signalling dependent (Fig. 2k). Compared to p14/p16 and p15 loci, we observed a different binding pattern of epigenetic regulators on p21 and p57 loci. Analysis of their binding at the SMAD2/3 binding sites indicated that SAP18, EZH1, EED, SNW1 and DPY30 bind to p21 and p57 loci, and their binding is decreased upon Activin A/TGFβ-SMAD2/3 signalling inhibition by SB431542 (Fig. 2l). On the other hand, SUV39H1, BAZ2A, DNMT1, and MECP2 were not enriched on p21 and p57 loci (Fig. 2l).

Next, we analysed the presence of histone modifications and DNA methylation on these CDKI loci in CSCs. Firstly, the repressive H3K9me3 and 5meC marks are enriched on p14/p16 and p15 loci, whereas they were decreased by Activin A/TGFβ-SMAD2/3 signalling inhibition (Fig. 2m). Bivalent histone marks H3K4me3/H3K27me3 and also the activating H3K27ac are present on p21/p57 loci, and decreased upon Activin A/TGFβ-SMAD2/3 signalling inhibition with a concomitant increase in the heterochromatin mark H3K9me3 and 5meC DNA methylation signature (Fig. 2n). These results indicated that the corresponding factors regulate p21 and p57 expression through maintaining the poised or primed epigenetic state of these loci.

Since the activating bivalent H3K4me3 modification is deposited by the TrxG and the repressive bivalent H3K27me3 is deposited by the PRC2 complexes, whereas removal of H3K27ac mark occurs by the activity of SIN3A/HDAC complex, we decided to investigate it further on p21 and p57 loci. For this, we

performed a knockdown and overexpression of Histone deacetylase complex subunit SAP18 and splicing factor/transcriptional coactivator SNW1, which we identified as SMAD2/3 interacting factors in our proteomic experiments. The knockdown of SAP18 led to a proportion of cells that activated expression of p21, while the overexpression of SAP18 reduced Activin A-mediated induction of p21 expression (Fig. 2o). The knockdown of SNW1 led to the reduced Activin A-mediated induction of p21 expression, whereas the overexpression of SNW1 overexpression led to upregulation of p21 signal (Fig. 2o).

Collectively, these results indicate that CDKI loci are regulated by SMAD2/3-facilitated deposition of heterochromatin/DNA methylation marks on p14/p16/p15 loci, and bivalent marks on p21/p57 loci in CSCs.

Pharmacological inhibition of BAZ2A and SUV39H1 sensitises PDAC cells from pancreatic cancer patients to Gemcitabine treatment.

To gain insight to the interconnection of Activin A/TGFβ-SMAD2/3 signalling and CDKIs in PDAC patient-derived CSCs, we analysed gene expression of malignant cells in patient tumours at the single-cell level by using scRNA-seq data. We annotated the cell types in PDAC patient samples based on gene expression signatures, which revealed that the tumours from PDAC patients contained epithelial cancer cells and also T-cells, myeloid cells, NK cells, fibroblasts, B-cells, endothelial cells, mast cells and neural cells (Fig. 3a-b). Since we were interested in malignant cells, we specifically further annotated the subpopulations of cancer cells (Fig. 3c). One subpopulation among the cancer cells (C2 cluster) had an elevated expression of several well-known CSC factors such as CD133 and PBX1 compared to other cancer cells (Fig. 3d), indicating that this subpopulation resembles CSCs present in our PDAC cell lines used in previous experiments. The PDAC patient CSCs had also a modest elevation of p21 and p57 compared to other PDAC cells and increased expression of ABCC3 that is involved in chemoresistance of CSCs due to the export of compounds such as gemcitabine out of the cell. This subpopulation also has elevated expression of factors usually found in pluripotent stem cells (OCT4, NANOG, SNON and SOX2) (Fig. 3d-e), and an elevated expression of central transcriptional inducers of EMT and positive regulators of cell motility (SNAI1, SNAI2, TWIST2, ZEB1, ZEB2) as well as other EMT factors (VEGFA, EVL, SPN, DAPK2, ETS1, RIPOR2, OGT, CCL4, CXCR4, CCL5, MALAT1, PTPRC, PLCG2, PIK3CG). Pathways based on top enrichment scores in the CSCs include “Response to TGFβ“, “stem cell proliferation”, “cell migration”, “Epithelial-to-Mesenchymal transition”, “G0 and Early G1”, and “POU5F1/OCT4, SOX2, NANOG repress genes related to differentiation” (Fig. 3f-g). Collectively, scRNA-seq analysis of PDAC patient tumours indicates the presence of cells that express pluripotency factors together with SMAD2/3 and show moderately elevated EMT/p21/p57/ABCC3 signatures compared to other cancer cells.

Next, we investigated the effect of Activin A/TGFβ-SMAD2/3 signalling on CDKI expression in PDAC patient tumour-derived CSCs. For this, we performed MACS separation of EPCAM+/CD133 + CSCs from three PDAC patient surgically isolated primary tumour samples. While qPCR analyses indicated that the expression of CDKIs is comparably low in CSCs compared to hPSCs, Activin A treatment of cells for 48h led to a significant induction of p21, p57, and p27 whereas there was induction in p15 in one of the

patient samples (Fig. 3h). Next, we investigated the effect of BAZ2A and SUV39H1 inhibition as well as the impact of Activin A/TGFβ signalling on chemosensitivity of patient PDAC cells. BAZ2A and SUV39H1 inhibitors led to the induction of apoptosis (Fig. 3i-j), whereas the co-treatment of cells with Gemcitabine (Gem) together with BAZ2A inhibitor BAZ2A-ICR or SUV39H1 inhibitor F5446 was more efficient in eliminating PDAC cells through apoptosis (Fig. 3i-j). Activin A/TGFβ-SMAD2/3 signalling increased the survival of PDAC cells to Gemcitabine treatment, whereas PDAC cells were sensitised to Gemcitabine treatment by BAZ2A and SUV39H1 inhibitor treatment (Fig. 3k).

Collectively, CDKIs are generally not extensively expressed in self-renewing CSCs, but Activin A signalling leads to an increase in p21, p27 and p57 expression in CSCs from patient tumours as observed in CSCs from PDAC cell lines. BAZ2A and SUV39H1 inhibitors sensitise patient PDAC cells to Gemcitabine treatment, thus indicating that the combination of Gemcitabine with BAZ2A/SUV39H1 inhibitors could improve the elimination of cancer cells, including CSCs.

SMAD2/3 cooperate with OCT4 and other pluripotency factors in CDKI regulation in CSCs.

Our results implied SMAD2/3 bind onto the regulatory regions in the proximity of p14/p16, p15, p18, p21, p27 and p57 loci in hPSCs and CSCs. Since SMAD2/3 cooperates with sequence-specific transcription factors in gene regulation [53], we hypothesised that SMAD2/3 might co-bind with other transcription factors to CDKI regulatory regions. By first performing transcription factor motif analyses within SMAD2/3 binding peaks we found the enrichment of OCT4, NANOG and SOX2 binding motifs at the SMAD2/3 peaks at CDKI regulatory regions, and ChIP-seq data analysis indicated the binding of OCT4, NANOG and SOX2 at the same genomic regions as SMAD2/3 in hPSCs (Fig. 4a).

While the core pluripotency factors OCT4, NANOG and SOX2 are robustly expressed in hPSCs, we also detect them in the CSC subpopulation (C2 cluster) in PDAC tumours (Fig. 3d-e), and OCT4, NANOG and SOX2 expression has been described in PDACs by other studies [19, 20]. Hence, we were interested in their possible function in the context of CDKI regulation in CSCs. ChIP-qPCR in CSCs showed binding of OCT4, NANOG and SOX2 on p21, p57, p14/p16 and p15 promoter regions shared with SMAD2/3 (Fig. 4b), revealing a similar binding in CSCs as in hPSCs. Sequential ChIP of OCT4 followed by SMAD2/3 showed that these stemness factors form a transcriptional complex on CDKI loci p14/p16, p15, p21, and p57 (Supplementary Fig. 2c).

In addition, SMAD2/3 and OCT4/NANOG/SOX2 share the same binding site with the epigenetic regulator SNON, which bound to the same genomic regions in the proximity of p21 and p57 loci, but was not enriched on p14/p16 and p15 loci (Fig. 4c). The SMAD2/3 repressor protein SNON/SKIL has been shown to suppress primitive streak and definitive endoderm genes in hPSCs, which helps to maintain pluripotency by suppressing differentiation [66]. Since SNON has an important function in regulating the decisions between self-renewal versus differentiation in hPSCs, which made its possible role in the context of CDKIs in CSCs interesting for us.

We found that SNON was recruited to p21 and p57 loci by SMAD2/3 in CSCs, since Activin A/TGFβ signalling inhibition with SB-431542 abolished the binding of SNON to p21 and p57 genomic regions (Fig. 4c). Our RNA-seq experiments of CSCs with Activin A/TGFβ and SB431542, had indicated the induction of SNON expression by Activin A/TGFβ signalling at the transcriptional level similarly to p21 and p57 thus indicating a regulatory circuitry (Fig. 2e). To further investigate this in CSCs, we used a SNON promoter-luciferase construct that has been shown to contain SMAD Binding Elements (SBEs) [54]. CSCs transfected with the SNON promoter-luciferase construct led to a robust signal, which was increased by Activin A treatment and strongly decreased by SB431542 after 24 hours (Fig. 4d). The SNON promoter containing site-specifically mutated SBEs (mtSBE) had a significantly lower luciferase signal in CSCs compared to the unmutated promoter-luciferase construct (Fig. 4d), underlining that SNON is directly induced by Activin A/TGFβ-SMAD2/3 in pancreatic CSCs. To estimate the relative importance of SMAD2/3 and OCT4/SOX2/NANOG on SNON expression in CSCs, we used the SNON promoter-luciferase construct mutated specifically at the SMAD2/3 binding site (mtSBE), OCT4/SOX2/NANOG (mtO/S/N) or both sites at the same time (Fig. 4e). While mtO/S/N led to a strong reduction of the luciferase signal in hPSCs, there was a more modest decrease in CSCs. On the other hand, mtSBE revealed a stronger signal reduction in CSCs compared to hPSCs, indicating that SMAD2/3 binding to SNON promoter has a more prominent regulatory role than OCT4/SOX2/NANOG in CSCs. Lastly, the combined mutation of both binding elements led to a near complete absence of luciferase signal in hPSCs, whereas some signal persisted in CSCs (Fig. 4f). This could indicate that additional factors contribute to the regulation of SNON in CSCs besides SMAD2/3 and OCT4/SOX2/NANOG. Moreover, SMAD2/3 ChIP-seq in CSCs and hPSCs indicated that SMAD2/3 bind to this common proximal promoter region at the transcription start site in both cell types (Fig. 4f). This suggested a regulatory circuitry in CSCs between Activin A/TGFβ-SMAD2/3 signalling and SNON in CSCs.

Co-immunoprecipitation of SMAD2/3 from the nuclear extracts of CSCs followed by western blotting indicated that SMAD2/3 form a protein complex OCT4, NANOG, SOX2 and SNON (Fig. 4g). Since SMAD2/3 and OCT4 bind to CDKI regulatory regions, we decided to explore the possible cooperation between SMAD2/3 and OCT4 on CDKI loci in CSCs by performing an inducible OCT4 knockdown in CSCs. OCT4 iKD led to the upregulation of p15, p21 p57 and p27 (Fig. 4h). SMAD2/3 and OCT4 CHIP-qPCR experiments in Scramble and OCT4 iKD cells indicated reduced SMAD2/3 and SNON binding to CDKI loci in the absence of OCT4 (Fig. 4i). We also observed a decrease in the repressive H3K27me3 bivalency mark on p15, p21, and p57 loci whereas the activating H3K4me3 bivalency mark showed no changes (Supplementary Fig. 2d).

Altogether, these data suggested that the SMAD2/3-OCT4-SNON complex maintains the characteristic CDKI expression pattern in CSCs. This could also include SOX2 and NANOG that cooperate together in a larger transcriptional complex, or mechanistically substitute for each other in regulating CDKIs in CSCs.

CDKI expression orchestrates self-renewal, G0 phase, EMT and chemoresistance of CSCs.

Having investigated the regulation of CDKI expression in CSCs, we next investigated the effects of p14, p16, p15, p21 and p57 in more detail. Colony formation assays of non-CSCs indicated a significant reduction in colony numbers and sizes (Fig. 5a), showing a general anti-proliferative effects on the bulk cancer cells, as expected. More importantly, CSC tumour sphere assays showed a reduction of CSC self-renewal capacity upon p14, p15 and p16 overexpression while p21 and p57 had no significant effects on CSC self-renewal (Fig. 5b and Supplementary Fig. 2e). However, CDKI overexpression slowed the proliferation of CSCs as revealed by reduced CSC sphere sizes also upon p21 and p57 OE (Fig. 5c). In addition, growth curve analyses indicated a slower proliferation of CSCs upon the overexpression of CDKIs whereas there was a growth inhibition by p14/p16/p15 OE as well as p21 and p57 OE (Fig. 5d).

To dissect the effects on cell cycle in live PDAC cells in more detail, we established a three-colour FUCCI system, which allows for the detection of cells in early G1, late G1, G1/S transition, S/G2/M and G0 phases (Fig. 5e-f). Using this FUCCI system in combination with CDKI overexpression we uncovered the lengthening of late G1 phase and an increase in cells that enter at least transitorily the G0 phase for p21 and p57 overexpression (Fig. 5g-h), but no increase in cell death (Fig. 5i). On the other hand, p14, p16 and p15 overexpression showed a lengthening of G1 phase and elevated cell death, but no increase in G0 phase cells (Fig. 5h).

Next, to determine the possible effects on CSC chemoresistance and sensitivity to cytotoxic treatments, we performed tumour sphere assays upon the overexpression CDKIs in the presence of Gemcitabine (Fig. 5j; Supplementary Fig. 2f). The overexpression of p15, p14 and p16 synergised with gemcitabine treatment and led to an efficient reduction of CSC sphere numbers and sphere sizes (Fig. 5j; Supplementary Fig. 2f). Interestingly, while we had not observed any considerable change in the number of CSC spheres and no detectable effect of CSC self-renewal capacity upon p21 and p57 overexpression, we noticed increased survival of CSCs if p21 and p57 are expressed upon Gemcitabine treatment (Fig. 5j). We hypothesised that this could be a consequence of a dual effect in CSCs: firstly, due to the lengthening of G1 phase or the entry into G0 phase, which can promote cell survival upon genotoxic insults caused by Gemcitabine. Secondly, the increase in SMAD2/3 transcriptional activity.

To test this hypothesis, we transfected FUCCI-CSCs with an SBE4 promoter-luciferase construct and after incubation for 24 hours, we FACS-sorted cells into distinct cell cycle phases to measure cell-cycle dependent SMAD2/3 transcriptional activity (Fig. 5k). These results indicated that SMAD2/3 shows fluctuations in activity depending on the cell cycle phase. SMAD mediated transcription is particularly active in G0 phase and early G1 (Fig. 5k). In concordance with these observations, p21 and p57 increase SMAD2/3 dependent transcriptional activity (Fig. 5l). Furthermore, overexpression of p15 and p21 increased the transcriptional activity of SMAD3 while CDKIs did not affect the transcriptional activity of SMAD3-EPSM which contains mutations at CDK4/6 phosphorylation sites (T178V, S203A, S207A, S212A; [55]) (Fig. 5m) suggesting that these linker residues mediate CDKI effects on SMAD2/3. Thus, CDKIs limit the activity of Cyclin D-CDK4/6 complexes, which concomitantly increases the length of the G1 phase and prevents inactivation of SMAD2/3. The resulting increase of SMAD2/3 transcriptional activity drives SMAD2/3-dependent cellular processes.

Lastly, we analysed the expression of genes pivotal for Epithelial-to-mesenchymal (EMT) transition (e.g., SNAI2, TWIST2) and gemcitabine resistance regulating ABC/multidrug-resistance genes (e.g., ABCC3), which are regulated by Activin A/TGFβ-SMAD2/3 signalling based on RNA-sequencing analyses, and bound by SMAD2/3 transcription factors based on SMAD2/3 ChIP-seq. We found that p21 and p57 overexpression lead also to the upregulation of SMAD2/3 target genes ABCC3, SNAI2 and TWIST2 in CSCs (Fig. 5n).

Collectively, our results indicate that SMAD2/3-OCT4 regulate p21 and p57 in CSCs, thus forming a positive feedback loop that can have impact CSC characteristics (Fig. 5o). The expression of these CDKIs leads to a lengthening of the G1 phase with transitory G0 phase together with the elevated expression of multidrug resistance gene ABCC3 and EMT master regulators SNAI2 and TWIST2. Collectively, this circuitry provides a protective effect on CSCs by supporting a quasi-mesenchymal cell state and increasing chemoresistance. In contrast, p14 and p16 reduce self-renewal of CSCs, increase apoptosis and slow PDAC cell proliferation with no beneficial effect to cancer cells.

SMAD2/3-SNON maintain p21 and p57 in a poised state with bivalent marks in CSCs.

Since our SMAD2/3 co-IP identified SNON as a cofactor in pancreatic CSCs and bound to p21 and p57 loci, we further investigated the function of SNON. Among the genes which showed elevated expression in CSCs together with SNON expression were EMT regulators ZEB1, ZEB2, SNAI1, SNAI2, and ABC/multidrug-resistance genes ABCC3 and ABCC4. These loci are bound by SMAD2/3, pluripotency factors OCT4 and NANOG, and they share overlapping binding regions with SNON (Fig. 6a). In addition, the loci exhibit bivalent H3K4me3 and H3K27me3 signatures similarly to p21 and p57 genes. To investigate the function of SNON in pancreatic CSCs, we performed knockdown of SNON in CSCs. This led to elevated p21 and p57 expression (Fig. 6b; Supplementary Fig. 2g), indicating that SNON could regulate the epigenetically poised state of these loci in pancreatic CSCs. SNON knockdown slowed PDAC cell growth (Fig. 6c), and it increased the late G1 and transitory G0 fraction of cells (Fig. 6d). SNON KD reduced CSC sizes but did not reduce CSC sphere numbers (Fig. 6e; Supplementary Fig. 2h). SNON KD also increased CSC chemoresistance to Gemcitabine (Fig. 6f-g). In contrast, the overexpression of SNON(1-366) which retains its ability to bind SMAD2/3 and is sufficient for transcriptional repression, but cannot be targeted by E3 ligases [56, 57], increased chemosensitivity of CSCs to Gemcitabine (Fig. 6h-i; Supplementary Fig. 2i).

Next, we investigated the effects on EMT and ABC transporter gene expression in CSCs. Knockdown of SNON resulted in elevated ABCC3, SNAI2 and TWIST2, and to a lesser extent the other markers (Fig. 6j-k) while SNO(1-366) overexpression reduced ABCC3, SNAI2 and TWIST2 expression in CSCs (Fig. 6l). Collectively, these data indicate that SNON regulates the expression of p21 and p57 loci as well as ABCC3, SNAI2 and TWIST2 in CSCs.

SMAD2/3-SNON and SMAD2/3-BAZ2A-SUV39H1 regulate enhancer-promoter looping in a locus-specific manner in CSCs.

In most cases, enhancers control gene expression through long-range interactions with promoters [48 49], but little is known about the enhancer/promoter connectome in pancreatic CSCs. To study the effects of SMAD2/3 and its coregulators on the enhancer/promoter connectome of CSCs, we performed H3K27ac In-situ ChIA-PET [50] experiments, which capture H3K27ac-centric chromatin interactions (i.e. enhancer/promoter connectome), and we analysed the enhancer-promoter looping at loci regulated by SMAD2/3-BAZ2A-SUV39H1 and SMAD2/3-SNON. We investigated specifically SNAI2 as an EMT gene, ABCC3 as a regulator of chemoresistance, as well as p14/p16 and p21 loci by 3C-qPCR to measure the relative abundance of enhancer-promoter connections on these loci.

First, we analysed the SNAI2 locus and uncovered the binding of SMAD2/3, SNON and OCT4 together with H3K27ac peaks at the enhancer and promoter loop anchors by ChIP-qPCR (Fig. 7a). While we had already confirmed the binding of SMAD2/3, SNON, and OCT4 on the promoter regions of SNAI2, ABCC3 and p12 locus, we investigated their binding also on the enhancer regions that represent the distant anchor sites that mediate the 3D enhancer-promoter chromatin looping. ChIP-qPCR indicated the enrichment of SMAD2/3, SNON and OCT4 on these distal enhancer regions, whereas the binding of SMAD2/3 and SNON was sensitive to SB431542 treatment at these regions, the binding of OCT4 was not affected (Fig. 7b). Next, we performed 3C-qPCR at the enhancer and promoter anchors for measuring the 3D looping and found that Activin A/TGFβ-SMAD2/3 signalling increases the promoter-enhancer contacts for SNAI2 locus whereas the pathway inhibitor SB431542 decreases these distant DNA contacts (Fig. 7c). We also examined the effects of SNON KD on enhancer-promoter connections at SNAI2 locus and uncovered that SNON KD leads to an increase in the 3D enhancer-promoter looping (Fig. 7d). The knockdown of OCT4 also increased the enhancer-promoter looping (Fig. 7e), indicating that both SMAD2/3 and OCT4 mediate the 3D chromatin structure at this EMT locus.

We performed a similar analysis of ABCC3 locus where we observed the binding of SMAD2/3, SNON and OCT4 together with H3K27ac peaks at the enhancer and promoter loop anchors, including the enhancer in the ABCC gene body selected for further analyses, and the anchor near ANKRD40 promoter region (Fig. 7f). A similar binding pattern for SMAD2/3, SNON and OCT4 was observed for the distant enhancers for ABCC3 and p21 loci (Fig. 7b). Activin A signalling, SNON KD and OCT4 KD increased the enhancer-promoter connections, suggesting that these factors mediate the 3D DNA looping at ABCC3 locus in CSCs (Fig. 7g-i). The p21 locus showed initial absence of looping but the treatment with Activin A led to the formation of an enhancer-promoter connection with a nearby control region, and the regulation of this interaction by SNON and OCT4, since their knockdown increased the Activin A effects (Fig. 7j-l).

In contrast to the SNAI2, ABCC3 and p21 loci, the p14/p16 locus revealed different regulatory mechanisms. 3D enhancer-promoter connections were not present in CSCs suggesting a repressed/silenced chromatin state on p14/p16 locus. On the other hand, nearby genes MTAP and MLLT3 indicated the binding of SMAD2/3, OCT4, NANOG and SOX2 to their regulatory regions (Supplementary Fig. 4a). We found that particularly MTAP shows a positive correlation of expression with p14/p16 and p15 genes, as well as a positive correlation with the Activin A ligand gene INHBA, and SMAD2/3 target gene SNON (Supplementary Fig. 4b-c). Therefore, we hypothesised that the MTAP

regulatory region could activate the expression of p14/p16, if the chromatin state of p14/p16 and p15 loci is derepressed in CSCs.

ChIP-qPCR showed the enrichment of SMAD2/3, SUV39H1, BAZ2A and OCT4 on the distal enhancer region, whereas the binding of SMAD2/3 and SNON was sensitive to SB431542 treatment at these regions, the binding of OCT4 was not affected (Fig. 7m). The stimulation or inhibition of Activin A/TGFβ-SMAD2/3 signalling did not drastically impact the establishment of 3D looping (Fig. 7n). However, the inhibition of SUV39H1 and BAZ2A led to an increase in the nearby enhancer looping with the p14/p16 locus (Fig. 7o). In addition, the knockdown of OCT4 facilitated new loop formation (Fig. 7p). These results indicate that SUV39H1 and BAZ2A mediate the repressed chromatin state of p14/p16 locus that can be derepressed by inhibiting SUV39H1 and BAZ2A.

Collectively, our results indicate that SUV39H1 and BAZ2A can be targeted by small molecule inhibitors for annihilating the CSC subpopulation in PDACs, thus providing a therapeutic strategy that could be used alone or in combination with current therapeutic regimens (Fig. 7q).

Discussion

In this study, we used pancreatic CSCs to uncover mechanisms regulating self-renewal. CSCs are able to self-renew and give rise to more differentiated cancer cells that ultimately make up the heterogeneous cell populations found in tumours. Pancreatic CSCs express some components of the pluripotency circuitry that controls the gene expression and epigenetic network that contributes to the stem cell-like characteristics of cancer cells [18].

Our small molecule compound screening experiments identified BAZ2A and SUV39H1 as attractive therapeutic targets for eliminating pancreatic CSCs. We showed that mechanistically, BAZ2A and SUV39H1 inhibition leads to the derepression of p14/p16 and p15 loci by a decrease in the repressive H3K9me3 mark and DNA methylation, allowing for p14/p16 and p15 upregulation. This blocks proliferation and self-renewal while increasing cell death. Since CSCs have lower sensitivity to chemotherapeutics besides their self-renewing capacity, we investigated the impact of BAZ2A and SUV39H1 inhibition on the chemoresistance of CSCs in combination with Gemcitabine treatment. We also showed that BAZ2A and SUV39H1 small molecule inhibitors can be combined with currently available PDAC chemotherapeutics such as Gemcitabine that upon combination led to synergistic elimination of CSCs. Thus, the combined treatment strategy could be particularly valuable for the subpopulation of PDAC patients who do not have p14/p16 and p15 genetic deletion but p14/p16 and p15 silencing through epigenetic means, which is estimated to occur approximately in up to half of PDAC patients. SUV39H1 regulates gene repression and heterochromatin formation, and due to its elevated expression in PDACs, it represents an intriguing novel mechanism for eliminating pancreatic CSCs. BAZ2A is very little studied in tumorigenesis, especially in pancreatic cancer, which makes it an attractive novel therapeutic target. In prostate cancer BAZ2A is overexpressed and is involved in maintaining prostate cancer cell growth [45, 46]. Interestingly, BAZ2A overexpression is also tightly associated with a

molecular subtype displaying a CpG island methylator phenotype (CIMP) [47, 72, 73], which could suggest an elevated silencing through repressive histone marks and DNA methylation of p14/p16 and p15 loci in pancreatic cancer. Collectively, our research discoveries will make it possible to use novel epigenetic machineries as therapeutic targets for specifically killing the harmful cancer-forming cells in patients.

By investigating the regulation of self-renewal in pancreatic CSCs, we found that the expression of CDKIs is actively regulated by an epigenetic mechanism. CDKIs in CSCs are maintained in a poised state (with the exception of p14/p16/p15 in CSCs) for rapid induction with distinct epigenetic marks that includes the bivalent H3K4me3/H3K27me3 signatures, and this is mediated by SMAD2/3-SNON cooperating with pluripotency factors OCT4 and/or NANOG and/or SOX2 and PRC2 and TrxG complexes. The encounter of elevated Activin/TGFβ allows for p21 and p57 induction. Interestingly, the expression of p21 and p57 has a protective effect on CSCs upon Gemcitabine treatment, which helps to understand why these CDKIs are not under strong selection for mutations/inactivation/deletions in PDACs. This is in contrast to p14/p16 and p15, which are more frequently homologously deleted or silenced by hypermethylation. We show that in PDACs where p14/p16 and p15 loci are not genetically deleted, the loci instead, tend to get silenced through transcriptional complexes between stem cell factors and SMAD2/3 cooperating with NoRC and SUV39H1 complexes. Collectively, our study uncovered a positive feedback loop that drives chemoresistance/partial EMT in CSCs.

The mechanisms uncovered by our current study could be relevant for a diversity of cell types in which the induction of CDKIs by TGFß will be not only important for blocking their proliferation but also for enhancing the activity of differentiation signals necessary for their final maturation/commitment. A decrease in CDKI expression is a common process in cancer and our results suggest that this mechanism could not only lead to increased capacity of proliferation but also control the EMT and chemoresistance of CSCs. Pancreatic CSCs express some components of the pluripotent stem cell circuitry including SOX2, OCT4 and NANOG in a subset of pancreatic cancer cells [19, 20]. Hence, the suppression of other CDKIs by SMAD2/3-SNON and these pluripotency factors with PcG/TrxG seems to support the self-renewal capacity of CSCs and control CDKI expression/EMT/chemoresistance through a similar mechanism by which NANOG-SMAD2/3-SNON maintains self-renewal in hPSCs [54]. A positive feedback loop helps the switch from a fully epithelial phenotype with faster CSC proliferation to a partial EMT with higher expression of multi-drug resistance genes (e.g., ABCC3 and ABCC4), and EMT master regulators (e.g., SNAI2 and TWIST2).

In our current study, we made use of a new fluorescent ubiquitination-based cell cycle indicator (FUCCI) system. The FUCCI is a powerful tool to assess cell cycle-dependent responsiveness to drugs and the effect of drugs, gene silencing or activation on the cell cycle without the need for synchronisation [58]. We have previously used the dual-colour FUCCI system in hESCs [51, 59, 60]. In our upgraded FUCCI system we used a truncated hCdt (DNA replication licensing factor) and Geminin (inhibitor of hCdt) to detect cells in G1, S and M-phases [60, 61], and in addition, the cell cycle inhibitor p27 with distinct site-specific mutations that characterises G0 cells [62]. This FUCCI system enables distinguishing between the cells in early G1,

late G1, early S, S/G2/M and G0 phases. Our results support the previous notions that cell cycle regulates the invasive behaviour of cells [63]. Cancer cells hijack developmental regulatory programs and signalling pathways to execute cell behaviors required for metastasis. Therefore, the same morphogenetic cell biological behaviors and molecular cues that are required for developmental processes such as gastrulation and neural crest delamination during embryogenesis are also utilized by tumor cells to proliferate, communicate with the surrounding microenvironment, and adopt an invasive phenotype [64]. While cancer progression is a disease of uncontrolled cell proliferation, cancer cell metastatic dissemination may require a switch from a proliferative to an invasive state. EMT in development and cancer progression indicates a strong association between loss of proliferation through downregulaton of mitotic cyclin/CDK activity and upregulation of CDKIs [65, 66]. In PDAC, epithelial, mesenchymal and partial EMT phenotypes have been observed. It has been found that partial EMT is associated with metastasis and cells can utilize diverse mechanisms of metastasis in pancreatic cancer. In pancreatic cancer and other cancer types the invading cells tend to express elevated levels of cell cycle inhibitors p21 and p27, and hence are predominantly in G0/G1 phase [63, 67]. The elevated TGFβ signalling activity found by us in the G0 phase indicates that cells residing in G0/G1 could be particularly effective for invasion due to the elevated expression of some EMT markers such as SNAI2 and TWIST2. Interestingly, due to the continuum of cell transition in the EMT process via transcriptional changes, PDAC cells are likely to possess invasive capacities that can include individual but also collective movement of cells during metastasis [68]. According to this report, the hybrid EMT state is characterised by co-expression of epithelial and mesenchymal genes, and low levels of EMT transcription factors. The carcinoma cells utilising partial EMT program migrate as clusters, whereas the cancer cells that undergo complete EMT mediated by transcriptional repression migrate as single cells. In support of this notion, partial EMT program is associated with high-grade poorly differentiated tumours, while complete EMT program is associated with low-grade well differentiated tumours [69].

The co-existence of epithelial and mesenchymal cells in PDACs is mediated by paracrine BMP signalling which stimulates EMT, and the BMP inhibitor GREM1 supports the epithelial phenotype [70]. Furthermore, CAF-secreted TGFβ1 activates MAPK and STAT3 signalling in PDAC cells to promote a partial EMT phenotype [71]. These findings are in concordance with our data showing that similarly to hPSC differentiation to endoderm via BMP and Activin A/TGFβ signalling, also CSCs respond to these developmental signalling pathways by shifting their cell cycle profile as well as EMT gene expression such as SNAI2 and TWIST2. Our data also indicate changes in cancer cell chemoresistance via ABCC3/4 expression. Of note, PDACs exhibit regional variations in stromal content as the tumour tissue contains “islands” of cancer cells surrounded by stromal fibroblasts, which can result in regional differences in cancer cells EMT characteristics.

Conclusions

We uncovered that BAZ2A and SUV39H1 cooperate with TGFβ/Activin-SMAD2/3 signalling to regulate stemness, cell cycle exit and chemoresistance in PDAC. SMAD2/3-OCT4-BAZ2A-SUV39H1 silences gene

expression including p14/p16/p15 genes, whereas SMAD2/3-SNON-OCT4 maintains a poised chromatin via enhancer-promoter looping on EMT and chemoresistance genes in CSCs. The identification of BAZ2A and SUV39H1 as regulators of CSC stemness in PDAC opens up new possibilities for targeted therapies that can eliminate CSCs and improve treatment outcomes for patients. This study contributes to a better understanding of the epigenetic mechanisms involved in CSC regulation, specifically in the context of pancreatic cancer (see Graphical Abstract).

MATERIALS AND METHODS

Supplementary Tables are included in Supplemental Information.

PDAC Cell lines and cell culture

The A13A cells were provided by Christine Iacobuzio-Donahue at The Memorial Sloan Kettering Cancer Center. FG and L3.6 were provided by Isaiah J. Fidler at The University of Texas MD Anderson Cancer Center. For standard cell cultures, cells were grown at 37°C humidified incubator containing 5% CO2 in Dulbeccos modified Eagles medium (DMEM), high glucose, GlutaMAX™ Supplement, pyruvate (Thermo Fisher Scientific, Inc.), 100 U/ml penicillin, 100 mg/ml streptomycin (Thermo Fisher Scientific, Inc.), MEM Non-Essential Amino Acids Solution 1X (Life Technologies; Thermo Fisher Scientific), MEM Vitamin Solution 1X (Life Technologies; Thermo Fisher Scientific) and 10% inactivated fetal calf serum (FCS; Life Technologies). For 3D cultures, cells we grown in ultra-low attachment plates (Thermo Fisher Scientific, Inc.) in Dulbecco's Modified Eagle Medium/F12 (Sigma-Aldrich) supplemented with 2.5mM L-Glutamine (Thermo Fisher Scientific, Inc.), 1 % B27 supplement (Life Technologies), 100 U/ml penicillin, 100 mg/ml streptomycin (Thermo Fisher Scientific, Inc.), 20ng/ml basic thermostable fibroblast growth factor (FGF-Basic TS, Proteintech) (5,000 cells/ml).

Tumour sphere assays

Cells are seeded into ultra-low attachment plates in Dulbecco's Modified Eagle Medium/F12 (Sigma-Aldrich) supplemented with 2.5mM L-Glutamine (Thermo Fisher Scientific, Inc.), 1 % B27 supplement (Life Technologies), 100 U/ml penicillin, 100 mg/ml streptomycin (Thermo Fisher Scientific, Inc.), 20ng/ml basic thermostable fibroblast growth factor (FGF-Basic TS, Proteintech) (5,000 cells/ml). For tumour sphere formation assay, cells were passaged after one-week incubation, and grown for another week after which the tumour sphere numbers were counted under a phase-contrast microscope using the 40x magnification lens or by Celigo Image Cytometer (Nexcelom). For RNA-seq and ATAC-seq experiments, serial passaging of the first-generation tumour spheres is required. After 7 days of incubation the tumour spheres were harvested by using a 40 µm cell strainer and centrifuged for 5 min at 200 x g at RT. Dissociate the pellet of tumour spheres to single cells using trypsin, and then expanded for another 4 days before performing the treatments of samples.

Knockin cell lines for Oct4

pCCC construct and OCT4 TALEN constructs (pTALEN_V2-OCT4F, pTALEN_V2-OCT4R) constructs were a gift from Francis C. Lynn and have been published [75]. OCT4-eGFP-PGK-Puro was a gift from Rudolf Jaenisch (Addgene plasmid #31937) and have been published [76]. Cells were transfected with Lipofectamine 3000 (ThermoFischer Scientific) and cultured for 4 days after transfection before selecting with 0.25 µg/mL puromycin (Sigma). Colonies were individually picked, trypsinized and placed into 24-well plates with 500 µl of media. Once clones were close to confluent, cells were replica plated for genotyping, freezing and for expanding the correctly targeted clones. Genomic DNA was extracted using Promega Wizard SV Genomic DNA Purification System (Promega) and genotyping was performed as described [75]. Positive clones were analysed by flow cytometry to estimate the frequency of eGFP positive cells in the cancer cell population. We additionally used primers GGTGCTCAGGTAGTGGTTGTCG and CTCTAATGTCCTCCTCTAACTGCTCTAGG for Oct4-GFP region verification, as well as CACAACCTCCCCTTCTACGAGC and GCATCATTGAACTTCACCTTCCCTC for Oct4-Puromycin region verification.

Generating INK4 and KIP/CIP Knockdown Cells

Previously validated shRNA expression vectors from Sigma-Aldrich (Supplementary Table 1) were transfected into H9 hPSCs with lipofectamine 2000 [60] and grown for 3 days. Cells were then cultured in the presence of puromycin until antibiotic-resistant colonies appeared. These were picked and characterized for knockdown efficiency.

Generating INK4 and KIP/CIP overexpressing Cells

For CDKI overexpression, cDNA sequences of p14, p15, p16, p18, p21, p27 and p57 were transferred into a pTP6 vector containing a CAG promoter. GFP and empty vector were used as controls. All inserts were confirmed by sequencing. Vectors were transfected into H9 hPSCs by lipofection [60] and grown for 3 days. Thereafter, cells with a stable integration were selected by continuous presence of puromycin. Individual clones were picked, propagated and used for subsequent analyses.

Cell culture of hESCs and FUCCI-hESCs lines

hESCs (H9 from WiCell) were grown in defined culture conditions as described previously [72]. H9 cells were passaged weekly using collagenase IV and maintained in chemically defined medium (CDM) supplemented with Activin A (10 ng/ml) and FGF2 (12 ng/ml). Pluripotent cells were maintained in Chemically Defined Media with BSA (CDM-BSA) supplemented with 10ng/ml recombinant human Activin A and 12ng/ml recombinant human FGF2 (both from Dr. Marko Hyvonen, Dept. of Biochemistry, University of Cambridge). Cells were passaged every 4-6 days with collagenase IV as clumps of 50-100 cells and dispensed at a density of 100-150 clumps/cm^2. The culture media was replaced 48 hours after the split and then every 24 hours. Alternative culture conditions were used to maintain hPSCs by maintaining cells on Vitronectin (StemCell Technologies)-coated plates in Essential 8 (E8) medium (Life technologies). Cells were passaged every 5-7 days using 0.5 uM EDTA and plated onto fresh vitronectin-

coated plates in E8 medium. Medium was refreshed every second day. This change corresponds to modification of protocols in our lab and has no influence on experimental outcomes. The generation of FUCCI-hESC lines has been described in [18] and are based on the FUCCI system described in [19].

In vitro differentiation of hESCs

FUCCI-hESCs were differentiated into endoderm as described previously [9]. Differentiation into endoderm was performed for up to 72 hours with a combination of cytokines as described in [59, 60]. For cells sorted by FACS, the cells were collected and immediately placed into the endoderm differentiation media. Endoderm specification was performed in CDM with polyvinyl Alcohol (CDM-PVA) prepared without insulin and supplemented with 50ng/ml FGF2, 1μM Ly-294002 (Promega), 100ng/ml Activin A, and 10ng/ml BMP4 (R&D) for 3 days. Alternatively, and for cells grown in E8 medium, H9 cells were plated as single cells onto gelatin/MEF-coated plates in E8 medium supplemented with 10uM Y-27632. The medium was refreshed the next day. Chemically Defined Media with Polyvinyl Alcohol (CDM-PVA) containing 100 ng/ml recombinant Activin A (CSCR, University of Cambridge), 80 ng/ml FGF2 (R&D Systems), 10 ng/ml BMP4 (CSCR, University of Cambridge), 10 μM LY29004 (Promega), and 3 μM CHIR99021 (Selleck Chemicals) was applied to the cells for 24 hours. The media was then replaced with fresh CDM-PVA supplemented with 100 ng/ml recombinant Activin A (CSCR, University of Cambridge), 80 ng/ml FGF2 (R&D Systems), 10 ng/ml BMP4 (CSCR, University of Cambridge) and 10 μM LY29004 (Promega). The next day, the media was removed and RPMI media supplemented with 1X B27 (Lifetech), 100 ng/ml Activin A, 80 ng/ml FGF2 and 1X non-essential amino acids (Lifetech) was added to the cells.

qPCR and Immunostaining

Methods for Q-PCR and immunostaining have been described previously [74]. Q-PCR data are presented as the mean of three independent experiments and error bars indicate standard deviations. Antibodies and primer sequences have been listed in Supplementary Table 2 and 3.

The small molecule screening library

The screening library contained concentrated small molecule compounds with verified biochemical activity against their targets. Most of the compounds target epigenetic regulators with high specificity (Supplementary Table 4).

Screening of the chemical compounds

The cells were grown in 96-well plates in standard growth medium with puromycin (1 μg/ml stock). Three technical replicates and three biological replicates were used for the screening. Cells were plated at a concentration of 10,000 cells in 100 μl of media per well in a 96-well plate. One day after plating the cells, the medium was changed to 90 μl standard growth medium supplemented with puromycin (0.5 μg/ml) and Activin A (10 ng/ml). On the same day, the compounds were added: first, 100x compound library dilutions were made, and 10uL of 100x diluted chemical was added to each well to obtain 1000x final

dilution of the compounds. Cells were then cultured with chemical compounds for five days with media change at day 0, day 2 and day 4 supplemented by fresh compounds. Each replicate was analyzed using Celigo Image Cytometer (Nexcelom) and flow cytometry. Cells were lifted and dissociated into single cells with Trypsin. Details on the antibodies that were used for flow cytometry are listed in Supplementary Table 5. The cells were incubated with 0.5 ug /ml final concentration of conjugated antibodies in 1% BSA-PBS for 40 minutes on ice and washing was repeated as before. The cells were then suspended in 300 uL 1% BSA-PBS with DAPI (1:2000) for live/dead separation and kept on ice to be used for the flow cytometry analysis.

Gene knockdown and overexpression

The stable knockdown and overexpression of SNON was performed by using previously published constructs [54] kindly provided by Prof. Ray Dunn at the Institute of Medical Biology, A*STAR (Agency for Science, Technology, and Research), Singapore. shRNA plasmid DNA was transfected into cells with Lipofectamine 3000 (Thermo Fischer Scientific) according to manufacturer guidelines. Puromycin was added to the growth media at 0.1ug/ml concentration and individual colonies were picked, expanded, and screened for gene knockdown compared to Scramble control transfected cells. SAP18 was knocked down and overexpressed with shRNA (h) Lentiviral Particles (sc-36454-V, Santa Cruz Biotechnology) and SAP18 lentiviral activation particles (sc-404214-LAC, Santa Cruz Biotechnology).

Nucleic acid extraction from cell lines

RNA was extracted using Direct-zol (TM) RNA extraction kit according to manufacturer protocol (Cambridge Bioscience, R2052). The quality of the RNA samples was verified using an RNA screen tape on a Tape-Station (Agilent). The RIN values for all samples were >7.5.

RNA Isolation and cDNA synthesis

Total RNA was isolated by RNeasy RNA Extraction Kit (Qiagen) according to manufacturer's guidelines. RNA was then eluted in 30µl of water and the concentration was measured using Nanodrop. The master mix was prepared as follows: 8µl 5x First-Strand Buffer (Invitrogen), 0.5µl Random primers (0.5 ug/ml) (Promega Cat. C1181), 1ul dNTP mix (10 mM each) (Promega Cat.U1515), 2 ul 0.1 M DTT, 0.5 ul RNase Out, 0.25 ul Superscript III Reverse Transcriptase (Life Technologies). 500 ng of total RNA into a separate tube with 11.75 ul RNase-free water. RNA was heated to 65 C for 5 min and allowed to chill on ice for 2 min. 8.25 ul of the master mix were added to RNA. The reaction was incubated at 25 C for 10 min and then at 42 C for 50 min. The reaction was then inactivated by heating at 70 for 15 min.

RT-qPCR

2ng of synthesized cDNA was added to 5µl Power SYBR Mix (Life Tecnologies, 4368708 (Master Mix)) and 1.5µl 2µM of forward and reverse primers. RT-qPCR was performed on ViiA 7 machine with the

following intervals: denaturation (95 C) for 15s and a total of 40 cycles, annealing/extension (60 C) for 60s, final extension (60 C) for 10 minutes.

Flow cytometry for cell cycle analysis

A13A and FG PDAC cells in which the FUCCI construct was incorporated were taken from adherent conditions and counted, then plated in spheroid conditions at a density of 5,000 cells / 1 mL medium for 10 days, before the cells were collected and analysed using Fortessa (BD Bioscience). Passaging was performed a day 5, after which cells were plated again in spheroid conditions, with the same initial density of 5,000 cells / 1 mL medium. Compounds were added in day 7, and the treatment lasted for 72 hours.Experiment was performed in 3 replicates. The data was analysed in FlowJo.

Preparation and Sequencing of Illumina RNA libraries

RNA-Seq libraries were created using the NEBNext Ultra RNA library prep kit using TruSeq indexes, following the manufacturer's recommendations. In summary, 500 ng of total RNA was used to isolate mRNA poly(A) by two rounds of purification using oligo dT magnetic beads followed by fragmentation and cDNA synthesis by random primers and reverse transcriptase. Bar-coded adapters were ligated to the cDNA fragments and a PCR reaction was performed to produce the sequencing libraries. To verify the library concentration and the library fragments length was used Agilent 2200 Tape-Station System. Adapter-ligated cDNA fragment libraries were sequenced on a NextSeq 500 platform (Illumina) using a paired-end run (2 × 41 bp).

RNA-sequencing analysis

Sequencing reads from the RNA-seq experiment were aligned to the human genome (hg38) using HISAT2 with the default parameters. FeatureCounts was used to assign mapped reads to genes with annotation gtf file Ensembl94. Differential gene expression analysis was performed using DESeq2 with IHW method for p value adjustment, apeglm method for effect size shrinkage, FDR-adjusted p value < 0.05 and log2 fold change > 0. Functional analysis of differential expressed genes was performed using Metacore. All plots were generated using R package 3.6.

Western blot analysis

Protein was isolated by lysing cells with RIPA Buffer (Sigma-Aldrich) supplemented by cOmplete EDTA-free protease inhibitor (Roche) and PhosSTOP™ (Sigma-Aldrich) and extracting the supernatant after high-speed centrifugation at 4°C. Protein quantification was performed using the Pierce BCA Protein Assay kit following the manufacturer's protocol. Isolated proteins were prepared for SDS-PAGE separation by dilution with 4× NuPAGE Sample buffer (Invitrogen), addition of NuPAGE™ Sample Reducing Agent ((10X), Invitrogen), 95°C for 5 minutes, and cooling. Isolated proteins were then analysed by Western blotting. Protein separation via SDS-PAGE was performed on a NuPAGE 4%–12% or 12% Bis-Tris gel (Life Technologies) with NuPAGE™ MOPS SDS Running Buffer (Life Technologies). Proteins were transferred

to a PVDF membrane, blocked with 5% milk in PBS and 0.05% tween 20, probed with protein-specific antibodies, incubated with horseradish peroxidase-conjugated secondary antibodies, and visualized via enhanced chemiluminescence using the SuperSignal West Pico Chemiluminescent Substrate (Thermo Scientific). All antibodies (Supplementary Table 6) were diluted in 5% milk in PBS and 0.05% tween 20. Quantification was performed using ImageJ gel analysis tool.

Immunostaining

The immunostaining method has been described previously [50, 59, 60]. Cells were fixed for 20 minutes at 4°C in PBS 4% PFA (electron microscopy grade), rinsed three times with PBS, and blocked and permeabilized at the same time for 30 minutes at room temperature using PBS with 10% Donkey Serum (Biorad) and 0.1% Triton X-100 (Sigma). Incubation with primary antibodies diluted in PBS 1% Donkey Serum 0.1% Triton X-100 was performed overnight at 4°C. Samples were washed three times with PBS, and then incubated with AlexaFluor secondary antibodies for 1 hour at room temperature protected from light. Cells were finally washed three times with PBS, and Hoechst (Sigma) was added to the first wash to stain nuclei. Images were acquired using a LSM 700 confocal microscope (Leica).

Chromatin Immunoprecipitation (ChIP)

All steps were performed on ice or at 4°C and ice-cold buffers and PBS were supplemented with 1mg/ml Leupeptin, 0.2mM PMSF, and 10mM NaButyrate were used unless otherwise stated. Approximately $5x10^6$ cells were used per sample and cross-linked with 1% formaldehyde for 15 minutes. Cross-linking was stopped by incubating samples with glycine at a final concentration of 0.125M for 5 minutes at room temperature, and the cells were washed with PBS followed by pelleting at 250g for 5 minutes. The pellet was re-suspended in 2ml ChIP Cell Lysis Buffer (CLB: 10 mM Tris pH8, 10 mM NaCl, 0.2% NP-40) and incubated for 10 minutes to lyse the plasma membranes. Nuclei were pelleted at 600g for 5 min, lysed in 1.25ml of ChIP Nuclear Lysis Buffer (NLB: 50 mM Tris pH8, 10mM EDTA, 1% SDS) for 10 minutes, and then 0.75ml of ChIP Dilution Buffer (DB: 20 mM Tris pH8, 2mM EDTA, 150mM NaCl, 0.01% SDS, 1% Triton X-100) was added to the samples. Chromatin was sonicated in 15ml Diagenode Bioruptor Pico water bath sonicator with an automated water cooling system, by performing 30 cycles of 30 seconds ON, 45 seconds OFF. This protocol resulted in the homogeneous generation of fragments of 100-400bp. Samples were clarified by centrifugation at 16000g for 10 minutes, and diluted with 3.5ml of DB. After pre-clearing with 10µg of non-immune IgG for 1h and 50µl of Protein G-Agarose for 2h, ChIP was performed overnight in rotation using specific antibodies (Table S2) or non-immune IgG as a control. After incubation for 1 hour with 30µl of Protein G-Agarose, beads were washed twice with ChIP Washing Buffer 1 (WB1: 20mM Tris pH8, 2mM EDTA, 50mM NaCl, 0.1% SDS, 1% Triton X-100), once with ChIP Washing Buffer 2 (WB2: 10mM Tris pH8, 1mM EDTA, 0.25M LiCl, 1% NP-40, 1% Deoxycholic acid), and twice with Tris-EDTA (TE: 10mM Tris pH8, 1mM EDTA). Precipitated DNA was eluted with 150µl of ChIP Elution Buffer (EB: 100mM $NaHCO_3$) twice for 15 minutes at room temperature in rotation, and processed as follows in parallel with 300 µl of sonicated chromatin non-used for ChIP (Input). Cross-linking was reverted by adding NaCl to a final concentration of 300mM for protein-DNA de-crosslinking and incubated

at 65°C for 5 hours and 1 µg RNase A (Sigma) to digest contaminating RNA. Finally, 60 µg of Proteinase K (Sigma) were added overnight at 45°C. DNA was extracted by sequential phenol-chloroform and chloroform extractions, and precipitated overnight at -80°C in 100mM NaAcetate, 66% ethanol and 50µg of glycogen (Ambion) as a carrier. After centrifugation at 16,000g for 1 hour at 4°C, DNA pellets were washed once with ice-cold 70% ethanol, and finally air dried. ChIP samples were resuspended in 30µl and 1:10 of the samples were used in qPCR for verifying the ChIP samples. Primers used for CHIP experiments are listed in Supplementary Table 7.

Chromatin Immunoprecipitation (ChIP) sequencing.

Tagmentation was performed on ChIPed DNA by Tn5 transposase from Nextera DNA Sample Prep Kit (Illumina, cat.#FC-121-1031). Tagmented DNA purified by DNA Clean & Concentrator-5 kit (Zymo research, Cat# 4013). Tagmented DNA was subjected to PCR amplification and double-size selection by AMPure XP beads (Beckman, cat.#A63881) (0.55x/0.9x). The library were multiplexed, quantified using a High-sensitivity d1000 TapeStation (Agilent) and then sequenced using a NextSeq 500 (Illumina) (paired-end, 2 × 41 bp). Sequencing depth was >20 million reads per sample.

Cell fractionations.

Cells were harvested with trypsin and washed twice with cold PBS. For cytoplasmic lysis, cells were suspended in 5 times packed cell volume (1 ul PCV = 10^6 cells) equivalent of Isotonic Lysis Buffer (10 mM Tris HCl, pH 7.5, 3 mM CaCl, 2 mM $MgCl_2$, 0.32 M Sucrose, Complete protease inhibitors and phosphatase inhibitors), and incubated for 12 min on ice. Triton X-100 was added to a final concentration of 0.3% and incubated for 3 min. The suspension was centrifuged for 5 min at 1,500 rpm at 4 °C and the supernatant (cytoplasmic fraction) transferred to a fresh chilled tube. For nuclear lysis, nuclear pellets were resuspended in 2 x PCV Nuclear Lysis Buffer+Triton X-100 (50 mM Tris HCl, pH 7.5, 100 mM NaCl, 50 mM KCl, 2 mM $MgCl_2$, 1 mM EDTA, 10% Glycerol, 0.3% Triton X-100, Complete protease inhibitors and phosphatase inhibitors) and dounce homogenized. The samples were incubated with gentle agitation for 30 min at 4 °C and then centrifuged with a Ti 70.1 rotor at 22,000 rpm for 30 min at 4 °C or with a Ti 45 rotor for 30 min at 20,000 rpm at 4 °C. The chromatin pellets were dounce homogenized in 2 x PCV Nuclear Lysis Buffer+Triton X-100 and Benzonase until the pellets gave much less resistance. The samples were incubated at RT for 30 min and centrifuged with either a Ti 70.1 rotor for 30 min at 22,000 rpm at 4 °C or with a Ti 45 rotor for 30 min at 20,000 rpm at 4 °C.

Protein co-immunoprecipitation.

Samples were incubated with 5 ug of cross-linked antibodies for 12h at 4 °C. Beads were washed five times with ten bead volumes of Nuclear Lysis Buffer and eluted in SDS western blotting buffer (30 mM Tris pH 6.8, 10% Glycerol, 2% SDS, 0.36 M beta-mercaptoethanol (Sigma), 0.02% bromophenol blue) by heating at 90 °C for 5 min. Samples were analysed by standard western blotting techniques.

Flow cytometry.

Flow cytometry was carried out with a BD MoFlo flow cytometer and analysed by FloJo software. Cell cycle distribution was analysed by Click-It EdU incorporation Kit (Invitrogen) according to manufacturer's guidelines. Marker expression was analysed at various timepoints during differentiation by first dissociating cells into single cells with Cell Dissociation Buffer (Gibco) and fixing in 4% PFA for 20 min at 4°C. This was followed by permeabilisation and blocking with 10% serum + 0.1% Triton X-100 in PBS for 30 min at RT and incubation with primary antibody in 1% serum + 0.1% Triton X-100 for 2h at 4°C. After washing the samples three times with PBS, they were incubated with a secondary antibody for 2h at 4°C, washed three times with PBS and analysed by flow cytometry.

Cell sorting by FACS

FACS on FUCCI-hESCs was performed as described before [18,19]. hESCs were washed with PBS and detached from the plate by incubating them for 10 min at 37 °C in Cell Dissociation Buffer (Gibco). Cells were then washed with cold filter sterilised 1% BSA in PBS, before incubating cells in PBS 1% BSA with Tra-1-60 primary antibody (1:100) and Alexa Fluor 647 donkey α-mouse secondary antibody (1:1000) on ice for 20 min in the dark with occasional gentle mixing. The cells were then washed once with at least 50x pellet volume PBS 1% BSA, resuspended gently in 3ml sterile maintenance media, and subjected to cell sorting by gating Tra-1-60+ cells according to the mAG/mKO2 FUCCI signals for hESCs or for mAG/mRFP/mKate2 FUCCI signals for PDAC cells. The cell sorting was performed with a BeckmanCoulter MoFlo MLS high-speed cell sorter by using parameters described previously [18], and the cells were sorted directly into collection tubes with 2 ml maintenance media.

Luciferase Assay

Cells were transfected with a SMAD2/3 reporter construct (SBE4-luciferase), Sox17 or GSC promoter constructs [77] and Renilla luciferase at a ratio of 10:1, using Lipofectamine 2000 (Invitrogen) [60]. Luciferase activity was measured with the dual luciferase assay kit following (Promega) manufacturer instructions. Firefly luciferase activity was normalized to Renilla luciferase activity for cell numbers and transfection efficiency. Samples were analyzed on a Glomax Luminometer and software.

EdU incorporation assay

Cell cycle distribution was analysed by Click-It EdU incorporation Kit (Invitrogen) according to manufacturer's guidelines. Flow cytometry was carried out with a BD MoFlo flow cytometer and analysed by FloJo software. Cells were cultured in media collected from cells with different treatment conditions for 72h, replacing the media every 24 hours.

3C-qPCR

The 3C-qPCR assay was conducted with modifications to a previously published method (Hagège et al 2007). Briefly, 5 million cells were fixed with 2% formaldehyde for 10 minutes at room temperature and subsequently lysed. In-situ digestion was performed using restrict enzyme AluI (New England Biolabs),

followed by ligation with T4 ligase (T4 ligase, New England Biolabs). The design of the 3C-qPCR primers employed a unidirectional strategy. Specifically, the primers were designed on the "forward" strand, positioned near the AluI restriction site (AGCT), within a range of 20 to 100 base pairs. Loading control primers for GAPDH were designed on the AluI fragment that does not overlap with the AluI restriction site. The primers for 3C-qPCR are as Supplementary Table 6.

Statistical analysis.

GraphPad Prism 6 was used for statistical analysis by performing t-test and two-way ANOVA tests followed by Bonferroni's corrected multiple comparisons between pairs of conditions. Unless otherwise indicated in the figure legends, we analysed three biological replicates for each data point in all graphs, and the level of significance was as follows: P< 0.1 (∗), P< 0.05 (∗∗), P< 0.01 (∗∗∗), and P< 0.001 (∗∗∗∗).

Abbreviations

PDAC	Pancreatic Ductal Adenocarcinoma
EMT	Epithelial-to-mesenchymal transition
CDKI	Cyclin Dependent Kinase Inhibitor
CDK	Cyclin Dependent Kinases
CSCs	Cancer Stem Cells
TGFβ	Transforming Growth Factor β
hPSCs	Human pluripotent stem cells
esBAF	ES cell-specific BAF
ncBAF	Non-canonical BAF
npBAF	Neural progenitor BAF
SSEA4	Stage-specific embryonic antigen-4
NoRC	Nucleolar remodeling complex
Gem	Gemcitabine
Ctrl	Control
Scr	Scramble
ns	Non-significant
pRb	Retinoblastoma protein
m/z	Mass-to-charge ratio
Mwt	Molecular weight
kDa	Kilodalton
KD	Knockdown
Ctrl	Control
Gem	Gemcitabine

Declarations

Ethical Approval and Consent to participate

Patient samples were obtained with consent and ethics permission (OCHRe ref: 21/A126, REC reference: 19/SC/0173; OCHRe ref: 19/A176, REC reference: 19/SC/0173) from Oxford Biobank.

Consent for publication

All authors have consented the publication. Patients have consented in the ethics permission (OCHRe ref: 21/A126, REC reference: 19/SC/0173; OCHRe ref: 19/A176, REC reference: 19/SC/0173) from Oxford Biobank.

Availability of supporting data

Further information and requests for resources and reagents should be directed to and will be fulfilled by the lead contact, Siim Pauklin (siim.pauklin@ndorms.ox.ac.uk).

Newly generated materials associated with the paper should be requested by contacting the lead contact. Data and code availability:

- RNA-seq dataset has been assigned GEO accession number GSE244327. Other data is available upon requests from the lead contact.
- This paper does not report original code.
- Any additional information required to reanalyze the data reported in this work paper is available from the lead contact upon request.

Competing interests

The authors declare no competing interests.

Funding

SP was supported by a Cancer Research UK Career Development Fellowship, Grant ID C59392/A25064, and Federation of European Biochemical Societies long-term fellowship. SWC was supported by the High-Level Talent Recruitment Programme for Academic and Research Platform Construction (Reference Number: 5000105) from Wenzhou-Kean University.

Authors' contributions

SM, FL, RN, MAM, MP, LC performed experiments, analysed the data, and contributed to the writing of the manuscript. SWC analysed and interpreted data and contributed to the writing of the manuscript. SP conceived the research, performed experiments, analysed the data, supervised the study and wrote the manuscript.

Acknowledgements

We are grateful to Prof Udo Oppermann, Dr Martin Philpott, and Dr James Dunford for help and support. We thank the flow cytometry and cell sorting staff at the NIHR BRC-Cambridge Phenotyping Hub at the University of Cambridge, the staff at the Botnar Research Centre at the University of Oxford, and the Flow Cytometry Facility at the MRC Weatherall Institute of Molecular Medicine at the University of Oxford.

Authors' information

There are no relevant additional information for authors.

References

1. Siegel, R., Naishadham, D. & Jemal, A. Cancer statistics, 2013. *CA Cancer J Clin* **63**, 11-30 (2013).
2. Ying, H. *et al.* Genetics and biology of pancreatic ductal adenocarcinoma. *Genes Dev* **30**, 355-385 (2016).
3. Rahib, L. *et al.* Projecting cancer incidence and deaths to 2030: the unexpected burden of thyroid, liver, and pancreas cancers in the United States. *Cancer Res* **74**, 2913-2921 (2014).
4. Perez-Mancera, P.A., Guerra, C., Barbacid, M. & Tuveson, D.A. What we have learned about pancreatic cancer from mouse models. *Gastroenterology* **142**, 1079-1092 (2012).
5. Kopp, J.L. *et al.* Identification of Sox9-dependent acinar-to-ductal reprogramming as the principal mechanism for initiation of pancreatic ductal adenocarcinoma. *Cancer cell* **22**, 737-750 (2012).
6. De La, O.J. *et al.* Notch and Kras reprogram pancreatic acinar cells to ductal intraepithelial neoplasia. *Proceedings of the National Academy of Sciences of the United States of America* **105**, 18907-18912 (2008).
7. Habbe, N. *et al.* Spontaneous induction of murine pancreatic intraepithelial neoplasia (mPanIN) by acinar cell targeting of oncogenic Kras in adult mice. *Proceedings of the National Academy of Sciences of the United States of America* **105**, 18913-18918 (2008).
8. von Figura, G. *et al.* The chromatin regulator Brg1 suppresses formation of intraductal papillary mucinous neoplasm and pancreatic ductal adenocarcinoma. *Nature cell biology* **16**, 255-267 (2014).
9. Pylayeva-Gupta, Y., Lee, K.E., Hajdu, C.H., Miller, G. & Bar-Sagi, D. Oncogenic Kras-induced GM-CSF production promotes the development of pancreatic neoplasia. *Cancer cell* **21**, 836-847 (2012).
10. Guerra, C. *et al.* Chronic pancreatitis is essential for induction of pancreatic ductal adenocarcinoma by K-Ras oncogenes in adult mice. *Cancer cell* **11**, 291-302 (2007).
11. Morris, J.P.t., Cano, D.A., Sekine, S., Wang, S.C. & Hebrok, M. Beta-catenin blocks Kras-dependent reprogramming of acini into pancreatic cancer precursor lesions in mice. *The Journal of clinical investigation* **120**, 508-520 (2010).
12. Puri, S., Folias, A.E. & Hebrok, M. Plasticity and dedifferentiation within the pancreas: development, homeostasis, and disease. *Cell stem cell* **16**, 18-31 (2015).
13. Ischenko, I., Petrenko, O. & Hayman, M.J. Analysis of the tumor-initiating and metastatic capacity of PDX1-positive cells from the adult pancreas. *Proceedings of the National Academy of Sciences of the United States of America* **111**, 3466-3471 (2014).
14. Topczewska, J.M. *et al.* Embryonic and tumorigenic pathways converge via Nodal signaling: role in melanoma aggressiveness. *Nat Med* **12**, 925-932 (2006).
15. Lonardo, E. *et al.* Nodal/Activin signaling drives self-renewal and tumorigenicity of pancreatic cancer stem cells and provides a target for combined drug therapy. *Cell stem cell* **9**, 433-446 (2011).
16. Pauklin, S. & Vallier, L. Activin/Nodal signalling in stem cells. *Development* **142**, 607-619 (2015).

17. Feng, Y., Liu, X. & Pauklin, S. 3D chromatin architecture and epigenetic regulation in cancer stem cells. *Protein Cell* **12**, 440-454 (2021).
18. Ervin, E.H., French, R., Chang, C.H. & Pauklin, S. Inside the stemness engine: Mechanistic links between deregulated transcription factors and stemness in cancer. *Semin Cancer Biol* **87**, 48-83 (2022).
19. Cho, J.H., Kim, S.A., Park, S.B., Kim, H.M. & Song, S.Y. Suppression of pancreatic adenocarcinoma upregulated factor (PAUF) increases the sensitivity of pancreatic cancer to gemcitabine and 5FU, and inhibits the formation of pancreatic cancer stem like cells. *Oncotarget* **8**, 76398-76407 (2017).
20. Lu, Y. *et al.* Knockdown of Oct4 and Nanog expression inhibits the stemness of pancreatic cancer cells. *Cancer Lett* **340**, 113-123 (2013).
21. Mouti, M.A. *et al.* KMT2A associates with PHF5A-PHF14-HMG20A-RAI1 subcomplex in pancreatic cancer stem cells and epigenetically regulates their characteristics. *Nat Commun* **14**, 5685 (2023).
22. Feng, Y. *et al.* BRD9-SMAD2/3 orchestrates stemness and tumorigenesis in pancreatic ductal adenocarcinoma. *bioRxiv* (2023).
23. French, R. & Pauklin, S. Epigenetic regulation of cancer stem cell formation and maintenance. *Int J Cancer* **148**, 2884-2897 (2021).
24. Sherr, C.J. & Roberts, J.M. CDK inhibitors: positive and negative regulators of G1-phase progression. *Genes Dev* **13**, 1501-1512 (1999).
25. Lim, S. & Kaldis, P. Cdks, cyclins and CKIs: roles beyond cell cycle regulation. *Development* **140**, 3079-3093 (2013).
26. Polyak, K. *et al.* p27Kip1, a cyclin-Cdk inhibitor, links transforming growth factor-beta and contact inhibition to cell cycle arrest. *Genes Dev* **8**, 9-22 (1994).
27. Besson, A. *et al.* Discovery of an oncogenic activity in p27Kip1 that causes stem cell expansion and a multiple tumor phenotype. *Genes Dev* **21**, 1731-1746 (2007).
28. Toyoshima, H. & Hunter, T. p27, a novel inhibitor of G1 cyclin-Cdk protein kinase activity, is related to p21. *Cell* **78**, 67-74 (1994).
29. Ryan, D.P., Hong, T.S. & Bardeesy, N. Pancreatic adenocarcinoma. *N Engl J Med* **371**, 1039-1049 (2014).
30. Liu, X.L., Ding, J. & Meng, L.H. Oncogene-induced senescence: a double edged sword in cancer. *Acta Pharmacol Sin* **39**, 1553-1558 (2018).
31. Bardeesy, N. *et al.* Both p16(Ink4a) and the p19(Arf)-p53 pathway constrain progression of pancreatic adenocarcinoma in the mouse. *Proceedings of the National Academy of Sciences of the United States of America* **103**, 5947-5952 (2006).
32. Aguirre, A.J. *et al.* Activated Kras and Ink4a/Arf deficiency cooperate to produce metastatic pancreatic ductal adenocarcinoma. *Genes Dev* **17**, 3112-3126 (2003).
33. Muniz, V.P. *et al.* The ARF tumor suppressor inhibits tumor cell colonization independent of p53 in a novel mouse model of pancreatic ductal adenocarcinoma metastasis. *Mol Cancer Res* **9**, 867-877

(2011).

34. Balli, D., Rech, A.J., Stanger, B.Z. & Vonderheide, R.H. Immune Cytolytic Activity Stratifies Molecular Subsets of Human Pancreatic Cancer. *Clinical cancer research : an official journal of the American Association for Cancer Research* **23**, 3129-3138 (2017).
35. Tu, Q. *et al.* CDKN2B deletion is essential for pancreatic cancer development instead of unmeaningful co-deletion due to juxtaposition to CDKN2A. *Oncogene* **37**, 128-138 (2018).
36. Villodre, E.S., Kipper, F.C., Pereira, M.B. & Lenz, G. Roles of OCT4 in tumorigenesis, cancer therapy resistance and prognosis. *Cancer Treat Rev* **51**, 1-9 (2016).
37. Hermann, P.C. *et al.* Distinct populations of cancer stem cells determine tumor growth and metastatic activity in human pancreatic cancer. *Cell stem cell* **1**, 313-323 (2007).
38. Maeda, S. *et al.* CD133 expression is correlated with lymph node metastasis and vascular endothelial growth factor-C expression in pancreatic cancer. *Br J Cancer* **98**, 1389-1397 (2008).
39. Kim, J. *et al.* An iPSC line from human pancreatic ductal adenocarcinoma undergoes early to invasive stages of pancreatic cancer progression. *Cell reports* **3**, 2088-2099 (2013).
40. Chen, P. *et al.* Discovery and Characterization of GSK2801, a Selective Chemical Probe for the Bromodomains BAZ2A and BAZ2B. *J Med Chem* **59**, 1410-1424 (2016).
41. Drouin, L. *et al.* Structure enabled design of BAZ2-ICR, a chemical probe targeting the bromodomains of BAZ2A and BAZ2B. *J Med Chem* **58**, 2553-2559 (2015).
42. Jiang, H. *et al.* Chaetocin: A review of its anticancer potentials and mechanisms. *Eur J Pharmacol* **910**, 174459 (2021).
43. Weirich, S., Khella, M.S. & Jeltsch, A. Structure, Activity and Function of the Suv39h1 and Suv39h2 Protein Lysine Methyltransferases. *Life (Basel)* **11** (2021).
44. Padeken, J., Methot, S.P. & Gasser, S.M. Establishment of H3K9-methylated heterochromatin and its functions in tissue differentiation and maintenance. *Nat Rev Mol Cell Biol* **23**, 623-640 (2022).
45. Mayer, C., Neubert, M. & Grummt, I. The structure of NoRC-associated RNA is crucial for targeting the chromatin remodelling complex NoRC to the nucleolus. *EMBO Rep* **9**, 774-780 (2008).
46. Mayer, C., Schmitz, K.M., Li, J., Grummt, I. & Santoro, R. Intergenic transcripts regulate the epigenetic state of rRNA genes. *Molecular cell* **22**, 351-361 (2006).
47. Gu, L. *et al.* BAZ2A (TIP5) is involved in epigenetic alterations in prostate cancer and its overexpression predicts disease recurrence. *Nature genetics* **47**, 22-30 (2015).
48. Lu, C. *et al.* SUV39H1 Represses the Expression of Cytotoxic T-Lymphocyte Effector Genes to Promote Colon Tumor Immune Evasion. *Cancer Immunol Res* **7**, 414-427 (2019).
49. Feoli, A. *et al.* Lysine methyltransferase inhibitors: where we are now. *RSC Chem Biol* **3**, 359-406 (2022).
50. Bertero, A. *et al.* Activin/nodal signaling and NANOG orchestrate human embryonic stem cell fate decisions by controlling the H3K4me3 chromatin mark. *Genes Dev* **29**, 702-717 (2015).

51. Madrigal, P. *et al.* Epigenetic and transcriptional regulations prime cell fate before division during human pluripotent stem cell differentiation. *Nat Commun* **14**, 405 (2023).
52. Blanco, E., Gonzalez-Ramirez, M., Alcaine-Colet, A., Aranda, S. & Di Croce, L. The Bivalent Genome: Characterization, Structure, and Regulation. *Trends in genetics : TIG* **36**, 118-131 (2020).
53. Zwijsen, R.M. *et al.* CDK-independent activation of estrogen receptor by cyclin D1. *Cell* **88**, 405-415 (1997).
54. Tsuneyoshi, N. *et al.* The SMAD2/3 corepressor SNON maintains pluripotency through selective repression of mesendodermal genes in human ES cells. *Genes Dev* **26**, 2471-2476 (2012).
55. Kretzschmar, M., Doody, J., Timokhina, I. & Massague, J. A mechanism of repression of TGFbeta/ Smad signaling by oncogenic Ras. *Genes Dev* **13**, 804-816 (1999).
56. Stroschein, S.L., Bonni, S., Wrana, J.L. & Luo, K. Smad3 recruits the anaphase-promoting complex for ubiquitination and degradation of SnoN. *Genes Dev* **15**, 2822-2836 (2001).
57. Stroschein, S.L., Wang, W., Zhou, S., Zhou, Q. & Luo, K. Negative feedback regulation of TGF-beta signaling by the SnoN oncoprotein. *Science* **286**, 771-774 (1999).
58. Singh, A.M., Trost, R., Boward, B. & Dalton, S. Utilizing FUCCI reporters to understand pluripotent stem cell biology. *Methods* **101**, 4-10 (2016).
59. Pauklin, S., Madrigal, P., Bertero, A. & Vallier, L. Initiation of stem cell differentiation involves cell cycle-dependent regulation of developmental genes by Cyclin D. *Genes Dev* **30**, 421-433 (2016).
60. Pauklin, S. & Vallier, L. The cell-cycle state of stem cells determines cell fate propensity. *Cell* **155**, 135-147 (2013).
61. Sakaue-Sawano, A. *et al.* Visualizing spatiotemporal dynamics of multicellular cell-cycle progression. *Cell* **132**, 487-498 (2008).
62. Oki, T. *et al.* A novel cell-cycle-indicator, mVenus-p27K-, identifies quiescent cells and visualizes G0-G1 transition. *Scientific reports* **4**, 4012 (2014).
63. Kohrman, A.Q. & Matus, D.Q. Divide or Conquer: Cell Cycle Regulation of Invasive Behavior. *Trends Cell Biol* **27**, 12-25 (2017).
64. Aiello, N.M. & Stanger, B.Z. Echoes of the embryo: using the developmental biology toolkit to study cancer. *Dis Model Mech* **9**, 105-114 (2016).
65. Iordanskaia, T. & Nawshad, A. Mechanisms of transforming growth factor beta induced cell cycle arrest in palate development. *J Cell Physiol* **226**, 1415-1424 (2011).
66. Vega, S. *et al.* Snail blocks the cell cycle and confers resistance to cell death. *Genes Dev* **18**, 1131-1143 (2004).
67. Qian, L.W. *et al.* Radiation-induced increase in invasive potential of human pancreatic cancer cells and its blockade by a matrix metalloproteinase inhibitor, CGS27023. *Clinical cancer research : an official journal of the American Association for Cancer Research* **8**, 1223-1227 (2002).
68. Carstens, J.L. *et al.* Stabilized epithelial phenotype of cancer cells in primary tumors leads to increased colonization of liver metastasis in pancreatic cancer. *Cell reports* **35**, 108990 (2021).

69. Aiello, N.M. *et al.* EMT Subtype Influences Epithelial Plasticity and Mode of Cell Migration. *Dev Cell* **45**, 681-695 e684 (2018).
70. Lan, L. *et al.* GREM1 is required to maintain cellular heterogeneity in pancreatic cancer. *Nature* **607**, 163-168 (2022).
71. Ligorio, M. *et al.* Stromal Microenvironment Shapes the Intratumoral Architecture of Pancreatic Cancer. *Cell* **178**, 160-175 e127 (2019).
72. Santoro, R., Li, J. & Grummt, I. The nucleolar remodeling complex NoRC mediates heterochromatin formation and silencing of ribosomal gene transcription. *Nature genetics* **32**, 393-396 (2002).
73. Dalcher, D. *et al.* BAZ2A safeguards genome architecture of ground-state pluripotent stem cells. *The EMBO journal* **39**, e105606 (2020).
74. Vallier, L. *et al.* Signaling pathways controlling pluripotency and early cell fate decisions of human induced pluripotent stem cells. *Stem Cells* **27**, 2655-2666 (2009).
75. Krentz, N.A., Nian, C. & Lynn, F.C. TALEN/CRISPR-mediated eGFP knock-in add-on at the OCT4 locus does not impact differentiation of human embryonic stem cells towards endoderm. *PloS one* **9**, e114275 (2014).
76. Hockemeyer, D. *et al.* Genetic engineering of human pluripotent cells using TALE nucleases. *Nat Biotechnol* **29**, 731-734 (2011).
77. Brown, S. *et al.* Activin/Nodal signaling controls divergent transcriptional networks in human embryonic stem cells and in endoderm progenitors. *Stem Cells* **29**, 1176-1185 (2011).

Figures

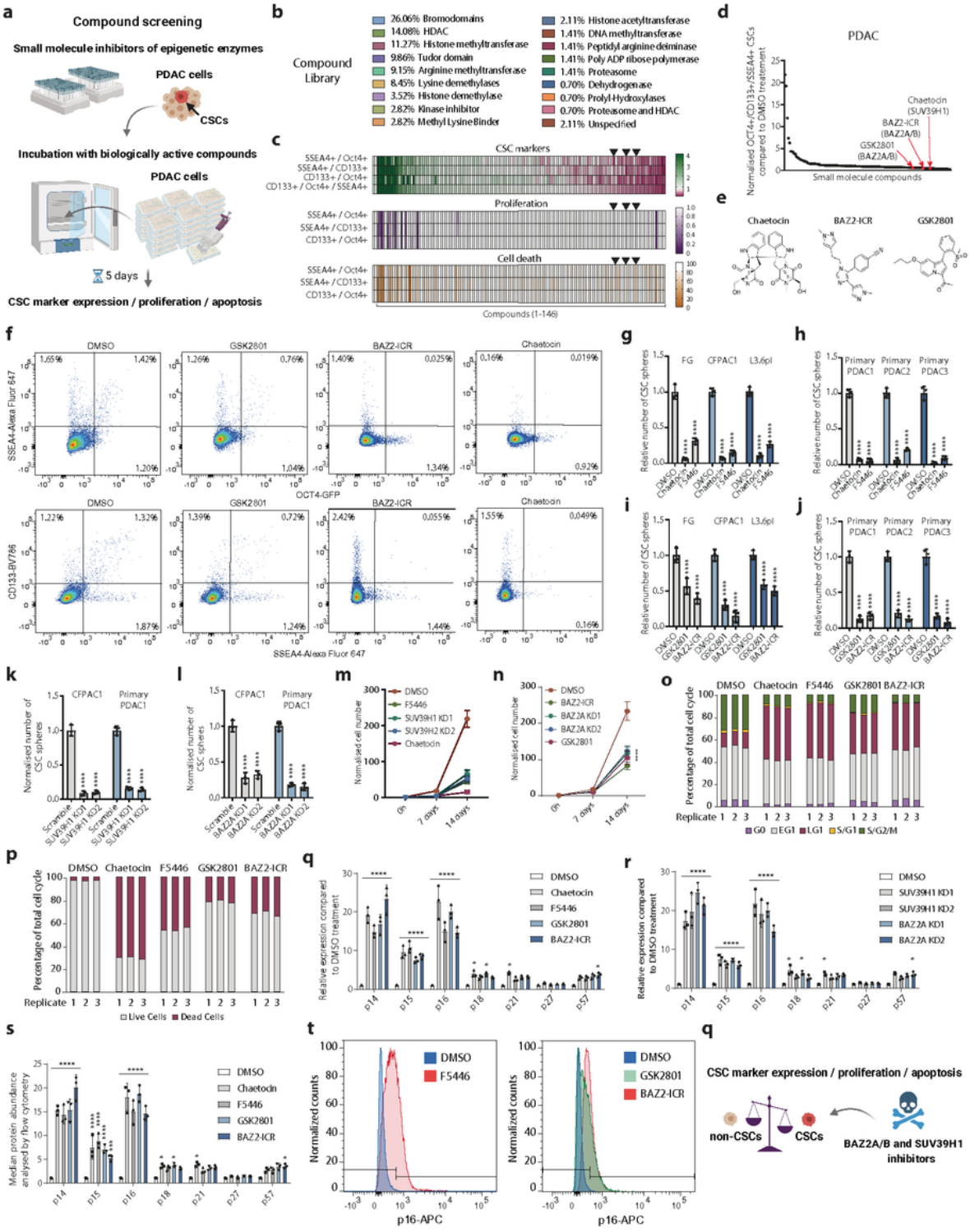

Figure 1

Chemical screening identifies BAZ2A and SUV39H1 are therapeutic targets for eliminating pancreatic CSCs. (**A**) Schematic depiction of the small molecule compound screening process on pancreatic cancer cells. (**B**) The classification of the compound library based on the percentage of the 142 compounds belonging to each class of enzymes they target. (**C**) BAZ2A and SUV39H1 inhibitors decrease the relative number of cells that express CSC markers OCT4-GFP, CD133 and SSEA4 as double positive cells or triple

positive cells. Heat maps of chemical screening depicting the relative change in the expression of CSC markers, cell numbers and cell viability. (**D**) BAZ2A and SUV39H1 inhibitors reduce the percentage of OCT4-GFP, CD133 and SSEA4 triple positive cells. (**E**) Chemical structures of BAZ2A inhibitors BAZ2-ICR, GSK2801, and SUV39H1 inhibitor Chaetocin. (**F**) Dot plots of samples treated with BAZ2A and SUV39H1 inhibitors and analysed by flow cytometry showing OCT4-GFP, CD133 and SSEA4 marker expression in pancreatic cancer cells. (**G-H**) SUV39H1 inhibition reduces CSC self-renewal in different PDAC cell lines and PDAC cells from surgically resected tumours. (**I-J**) BAZ2A inhibition reduces CSC self-renewal in different PDAC cell lines and PDAC cells from surgically resected tumours. (**K**) SUV39H1 knockdown reduces CSC self-renewal in PDAC cell line and primary tumour cells. (**L**) BAZ2A knockdown reduces CSC self-renewal in PDAC cell line and primary tumour cells. (**M**) SUV39H1 knockdown or chemical inhibition decreases PDAC cell proliferation. (**N**) BAZ2A knockdown or chemical inhibition decreases PDAC cell proliferation. (**O-P**) BAZ2A and SUV39H1 inhibitors lengthen the G1 phase and induce cell death. (**Q-T**) SUV39H1 and BAZ2A inhibitors and knockdown lead to p14, p16 and p15 upregulation at the (Q-R) mRNA level and (S-T) protein level. (**Q**) Schematic depiction showing that BAZ2A and SUV39H1 inhibition eliminates CSCs. Experiments represent three replicates. Statistical analysis was performed by 2-way ANOVA with multiple comparisons with Tukey correction and **** marks adjusted P-value <0.0001, *** is adjusted P-value <0.001, ** is adjusted P-value <0.01, * is adjusted P-value <0.05.

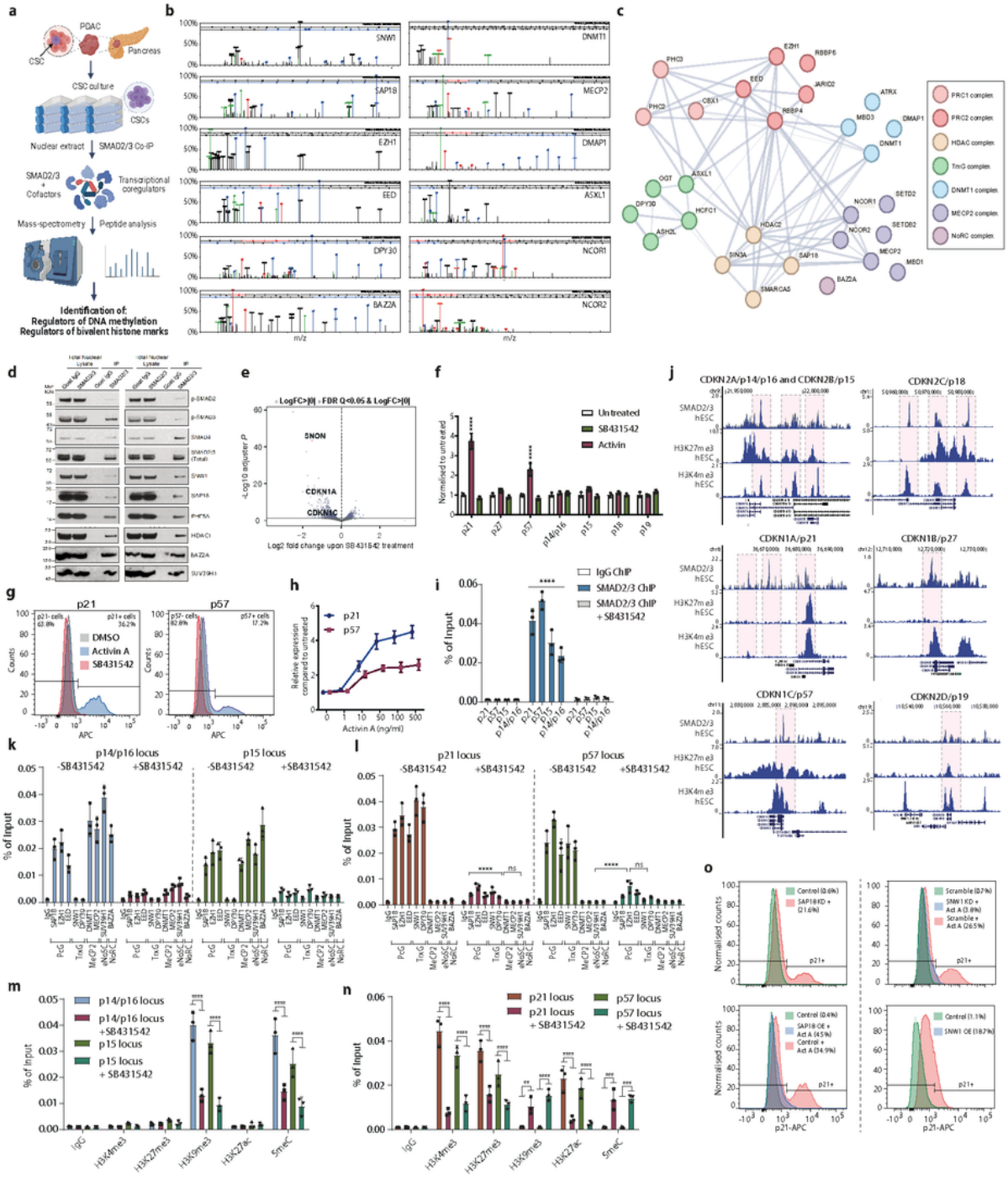

Figure 2

Identification of BAZ2A and SUV39H1 as SMAD2/3 interacting factors in CSCs. (**A**) Schematic overview of identifying SMAD2/3 interacting proteins by Co-IPs followed by mass-spectrometry in CSCs. (**B**) Peptide spectra of SMAD2/3 interacting epigenetic regulatory proteins identified by mass spectrometry. (**C**) STRING protein interaction network depiction of SMAD2/3 cofactors in CSCs. (**D**) Verification of SMAD2/3 interaction with BAZ2A, SUV39H1, SNW1 and SAP18 in CSCs from A13A and L3.6pl PDAC cell

lines. (**E-G**) SNON, p21 and p57 are upregulated by Activin/TGFβ signalling in pancreatic CSCs analysed by (**E**) RNA-seq, (**F**) qPCR, and (**G**) flow cytometry. (**H**) Activin A concentration effects on p21 and p57 induction in CSCs. (**I**) SMAD2/3 binds to p21, p57, p15 and p14/p16 loci in CSCs. (**J**) SMAD2/3 bind to CDKI loci in pluripotent cells. Histone H3K4me3 and H3K27me3 mark CDKI loci in pluripotent cells. (**K**) SAP18, EZH1, EED, DPY30 bind to p21 and p57 loci in an Activin/TGFβ signalling dependent manner, analysed by ChIP-qPCR. (**L**) DNMT1, MECP, SUB39H1 and BAZ2A bind to p14/p16 and p15 loci in an Activin/TGFβ signalling dependent manner, analysed by ChIP-qPCR. (**M**) H3K4me3, H3K27me3 and H3K27ac are replaced by more permanent repressive marks including H3K9me3 and 5meC on p21 and p57 loci. (**N**) H3K9me3 and 5meC repressive marks decrease on p14/p16 and p15 loci upon Activin/TGFβ signalling inhibition. (**O**) The knockdown and overexpression of SNW1 and SAP18 regulates p21 expression in CSCs as shown by flow cytometry analyses. Statistical analysis was performed by 2-way ANOVA with multiple comparisons with Tukey correction and **** marks adjusted P-value <0.0001, *** is adjusted P-value <0.001, ** is adjusted P-value <0.01, * is adjusted P-value <0.05.

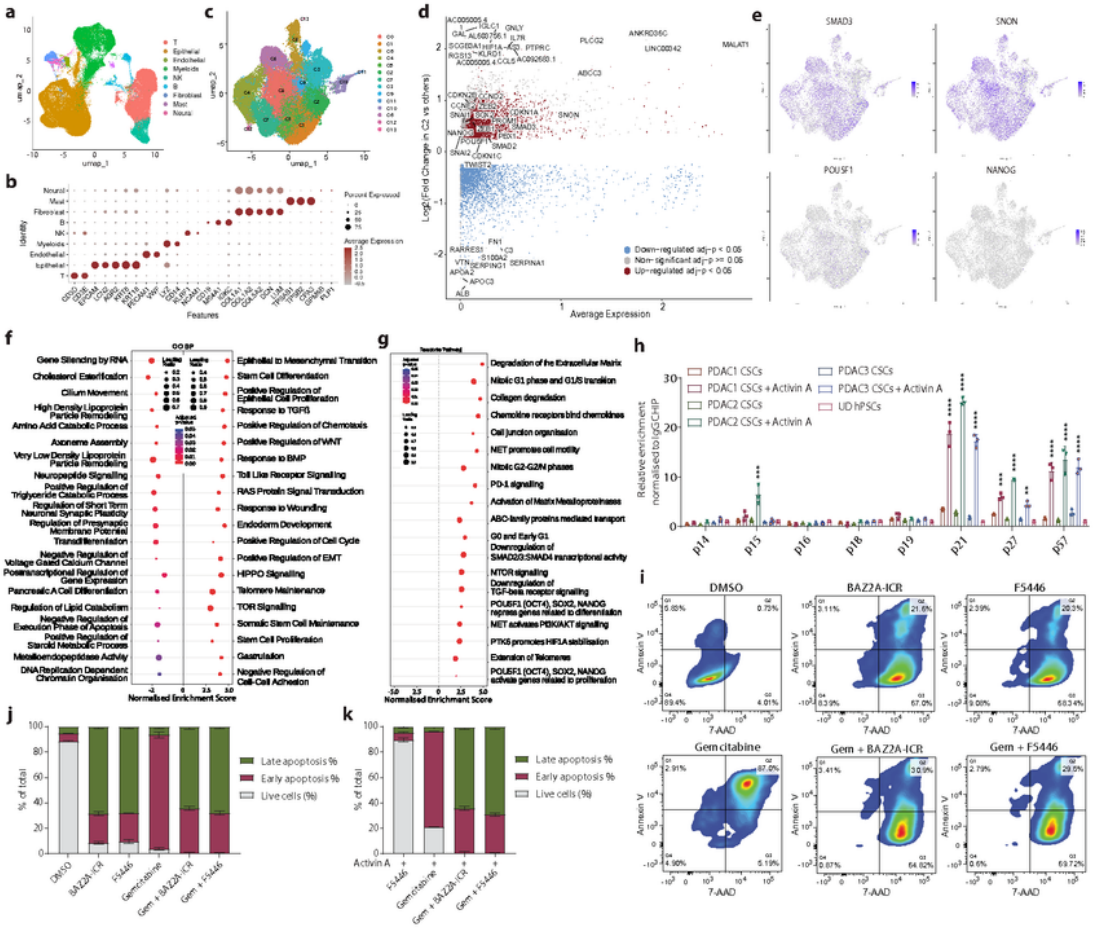

Figure 3

Activin/TGFβ signalling regulates CDKIs in PDAC patient derived CSCs. (**A-B**) Cell type annotation in PDAC patient tumour sample RNA-sequencing data. Epithelial cells mark cancer cells. (**C**) Subclustering of cancer cells based on PDAC patient tumour sample RNA-sequencing data. (**D**) Volcano plot of differentially expressed genes in C2 cluster of CSCs vs all other cancer cells in the PDAC tumours based on scRNA-sequencing data. Red colour shows significantly upregulated genes in C2 cluster and blue

shows significantly downregulated genes in Cs cluster, compared to all other cancer cells. (**E**) SMAD3, SNON, POU5F1, and NANOG expression in PDAC patient tumours based on single-cell RNA-sequencing. (**F-G**) Pathway enrichment analyses for top enrichment scores of RNA-seq data from PDAC patients with top and bottom quartile SNON expression based on (F) GO BP and (G) Reactome pathways. All shown pathways are statistically significant based on adj. p-values. (**H**) p21 and p57 are induced by elevated Activin/TGFβ signalling in CSCs isolated from primary PDACs from patients (n=3). (**I-J**) BAZ2A and SUV39H1 inhibition increases the chemosensitivity of PDAC cells to gemcitabine treatment leading to cell death. Apoptosis assays of cancer cells isolated from primary PDACs from patients (n=3). (**K**) Activin/TGFβ signalling increases PDAC cell chemoresistance to gemcitabine, whereas BAZ2A and SUV39H1 inhibition can reverse the Activin/TGFβ signalling effects. Apoptosis assays of cancer cells isolated from primary PDACs from patients (n=3). Statistical analysis was performed by 2-way ANOVA with multiple comparisons with Tukey correction and **** marks adjusted P-value <0.0001, *** is adjusted P-value <0.001, ** is adjusted P-value <0.01, * is adjusted P-value <0.05.

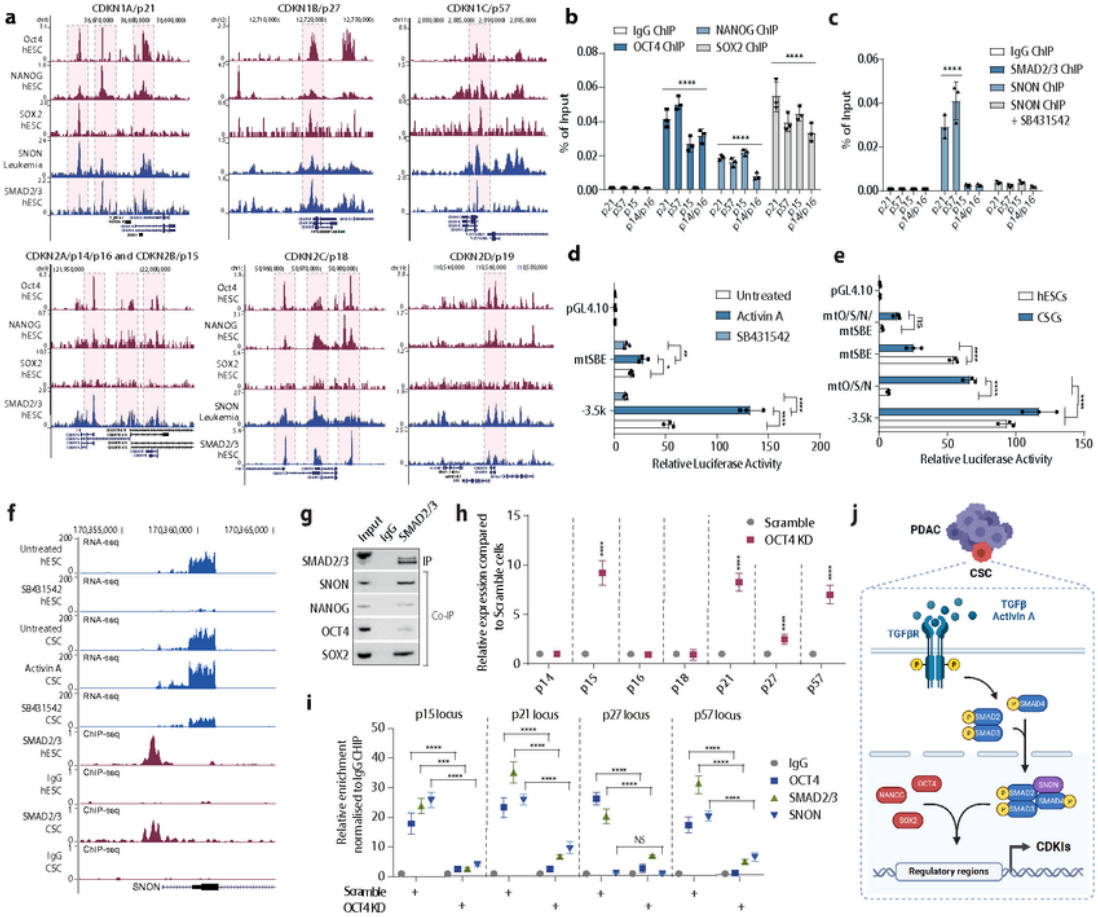

Figure 4

SMAD2/3-SNON cooperate with OCT4/NANOG/SOX2 in regulating CDKI expression. (**A**) SMAD2/3, OCT4, SOX2, NANOG bind to CDKI loci in pluripotent cells. Histone H3K4me3 and H3K27me3 mark CDKI loci in pluripotent cells. SNON data represents leukemia cells. (**B**) OCT4, NANOG and SOX2 bind to p21, p57, p14/p16 and p15 loci in CSCs. (**C**) SNON binding to p21, p57 loci depend on Activin/TGFβ signalling. (**D**) SNON promoter-luciferase assay shows the functionality of SMAD Binding Element in CSCs upon Activin

A of SB431542 treatment for 24h. (**E**) OCT4/NANOG/SOX2 binding sites and SBE regulate SNON expression in both hPSCs and CSCs as seen by SNON promoter-luciferase assays. (**F**) Snapshot of SNON/SKIL genomic locus showing RNA-seq and SMAD2/3 binding in hPSCs and CSCs. (**G**) SMAD2/3 protein interacts with co-repressor SnoN and the transcription factors NANOG, OCT4 and SOX2 in CSCs. SMAD2/3 was immunoprecipitated from the nuclear fractions of CSCs and analysed by western blotting. (**H**) OCT4 knockdown leads to an increase in p15, p21, p27 and p57 expression in CSCs. Scramble and OCT4 KD cells were analysed by Q-PCR for determining the expression of CDKIs. (**I**) OCT4 knockdown causes a decrease in repressive bivalent mark H3K27me3 on p15, p21, p27 and p57 loci. Scramble and NANOG KD cells were analysed by ChIP-QPCR of H3K4me3 and H3K27me3 marks on CDKI loci. Significant differences calculated by two-way ANOVA are marked. (**J**) Schematic depiction of Activin/TGFβ-SMAD2/3 signalling in cooperating with SNON and OCT4/NANOG/SOX2 in regulating the primed state of p21 and p57 by facilitating the deposition of bivalent histone marks. Statistical analysis was performed by 2-way ANOVA with multiple comparisons with Tukey correction and **** marks adjusted P-value <0.0001, *** is adjusted P-value <0.001, ** is adjusted P-value <0.01, * is adjusted P-value <0.05.

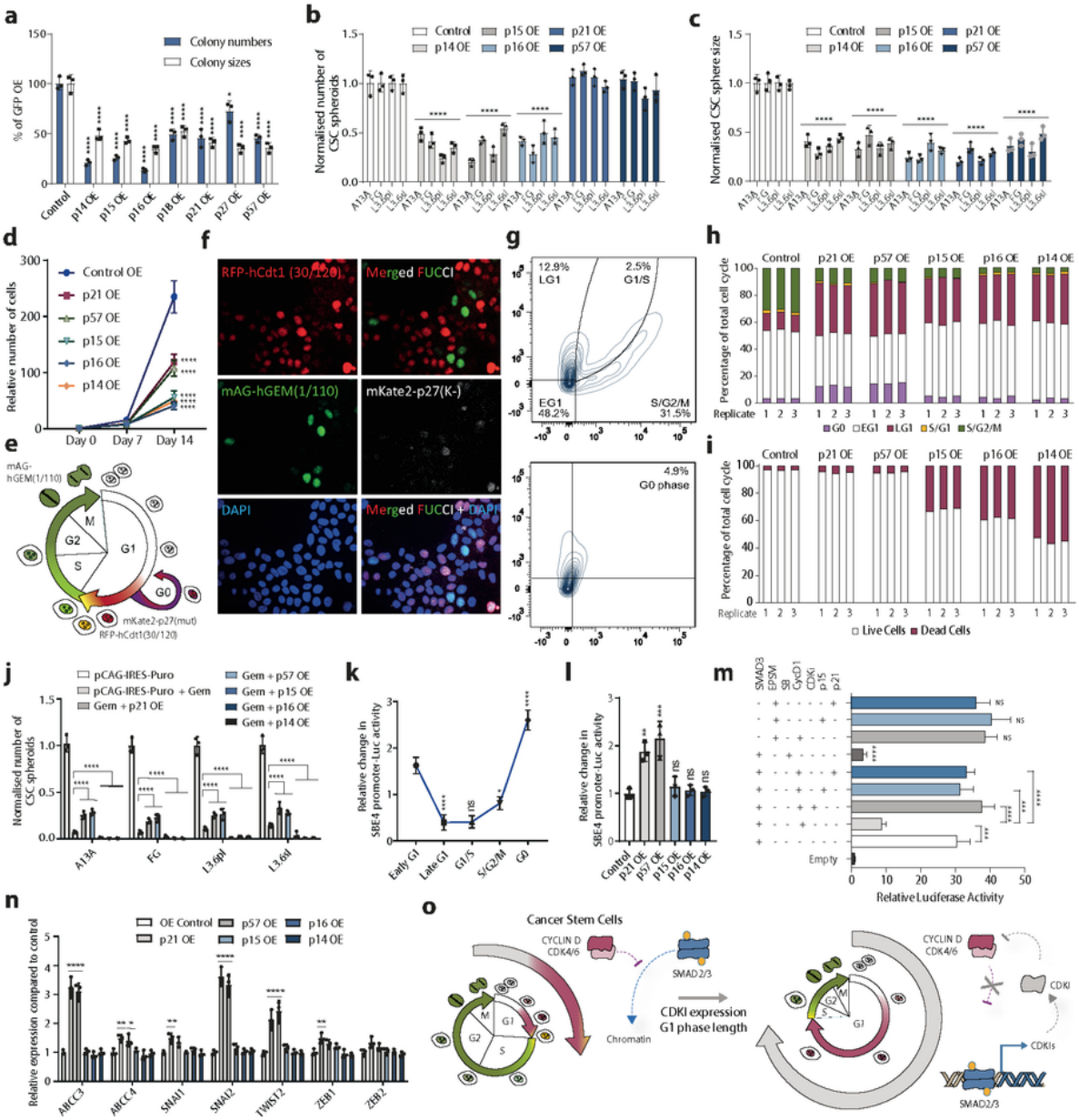

Figure 5

CDKI expression impacts G1 lengthening and G0 phase habitation, EMT, and chemoresistance of CSCs. (**A**) The number of PDAC cell colonies and colony sizes are reduced in cells overexpressing CDKIs compared to OE GFP cells. Significant differences compared to OE GFP calculated by t-test are marked. (**B**) Overexpression of p14/p15/p16 OE reduces CSC self-renewal capacity as indicated by the decrease in CSC sphere numbers. (**C**) Overexpression of all CDKIs slows CSC proliferation shown by the decrease in

CSC sphere sizes. (**D**) Overexpression of CDKIs slows PDAC cell proliferation shown by growth curve analyses. (**E-F**) Schematics and representative three-coloured FUCCI signals in PDAC cells visualised by immunofluorescence microscopy. (**G-H**) p21 and p57 overexpression extends the late G1 phase and increases G0 phase cells according to flow cytometry analyses. (**I**) p14/p15/p16 OE increases CSC apoptosis whereas p21 and p57 OE does not increase CSC apoptosis based on flow cytometry analyses. (**J**) p21 and p57 OE increases CSC resistance to Gemcitabine whereas p14, p15 and p16 OE decreases CSC resistance to Gemcitabine. (**K**) SMAD2/3 activity is highest in G0 phase CSCs measured by SBE4 promoter-luciferase assays in FUCCI-CSCs. (**L**) p21 OE and p57 OE increases SBE4 promoter-luciferase activity in CSCs. (**M**) CDKIs induce SMAD2/3 transcriptional activity via inhibiting Cyclin D-CDK4/6 mediated phosphorylation of SMAD2/3 in its linker region. Cells were co-transfected with CDKI expressing plasmids and a luciferase construct under the regulation of a consensus SMAD Binding Element. Significant differences calculated by t-test are marked. (**N**) p21 OE and p57 OE leads to ABCC3, SNAI2 and TWIST2 upregulation in CSCs. (**O**) Schematic depiction of the circuitry of SMAD2/3 and CDKIs that regulates the self-renewal and cell cycle progression of CSCs. SMAD2/3-SNON-OCT4 keep p21 and p57 in a poised state for rapid activation whereas p14/p16 are silenced. Elevated Activin/TGFβ signalling allows SMAD2/3 to activate CDKI expression, thus forming a positive regulatory loop. This circuitry involves CDK4/6 inhibition by CDKIs, which in turn hyper-activates SMAD2/3 dependent induction of CDKI expression that drive G1 phase lengthening and entry of G0 phase. Statistical analysis was performed by 2-way ANOVA with multiple comparisons with Tukey correction and **** marks adjusted P-value <0.0001, *** is adjusted P-value <0.001, ** is adjusted P-value <0.01, * is adjusted P-value <0.05.

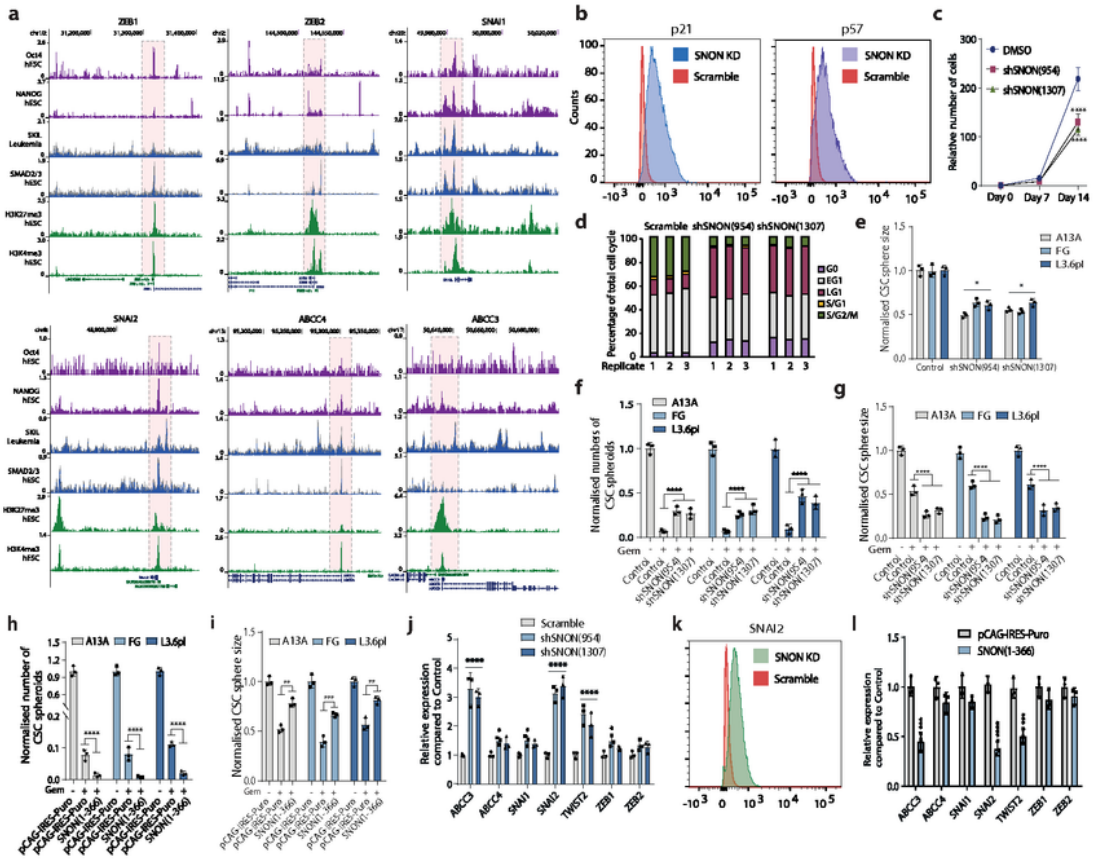

Figure 6

SNON regulates EMT inducers SNAI2, TWIST2 and chemoresistance transporter ABCC3 in CSCs. (**A**) Snapshots of genomic regions for EMT regulators and ABCC3/4 indicates SNON, SMAD2/3 and OCT4/NANOG/SOX2 binding with bivalent histone modifications in hPSCs. (**B**) SNON knockdown leads to p21 and p57 induction based on flow cytometry analyses. (**C**) SNON knockdown slows PDAC cell doubling. (**D**) SNON KD lengthens late G1 and increases G0 phase cells. (**E**) SNON KD lowers CSC sphere

size indicating slower proliferation. (**F**) SNON KD increases CSC chemoresistance upon Gemcitabine treatment as indicated by changed CSC numbers in tumour sphere assays. (**G**) SNON KD slows CSC self-renewal as indicated by smaller CSC spheres in tumour sphere assays. (**H**) SNON OE decreases CSC chemoresistance upon Gemcitabine treatment as revealed by decreased CSC numbers. (**I**) SNON OE increases CSC proliferation as revealed by increased CSC numbers in Gem treated cells. (**J**) SNON KD leads to increased ABCC3, SNAI2 and TWIST2 expression in CSCs. (**K**) SNAI2 expression in SNON KD analysed by flow cytometry. (**L**) SNON OE leads to decreased ABCC3, SNAI2 and TWIST2 expression analysed by qPCR analyses. Statistical analysis was performed by 2-way ANOVA with multiple comparisons with Tukey correction and **** marks adjusted P-value <0.0001, *** is adjusted P-value <0.001, ** is adjusted P-value <0.01, * is adjusted P-value <0.05.

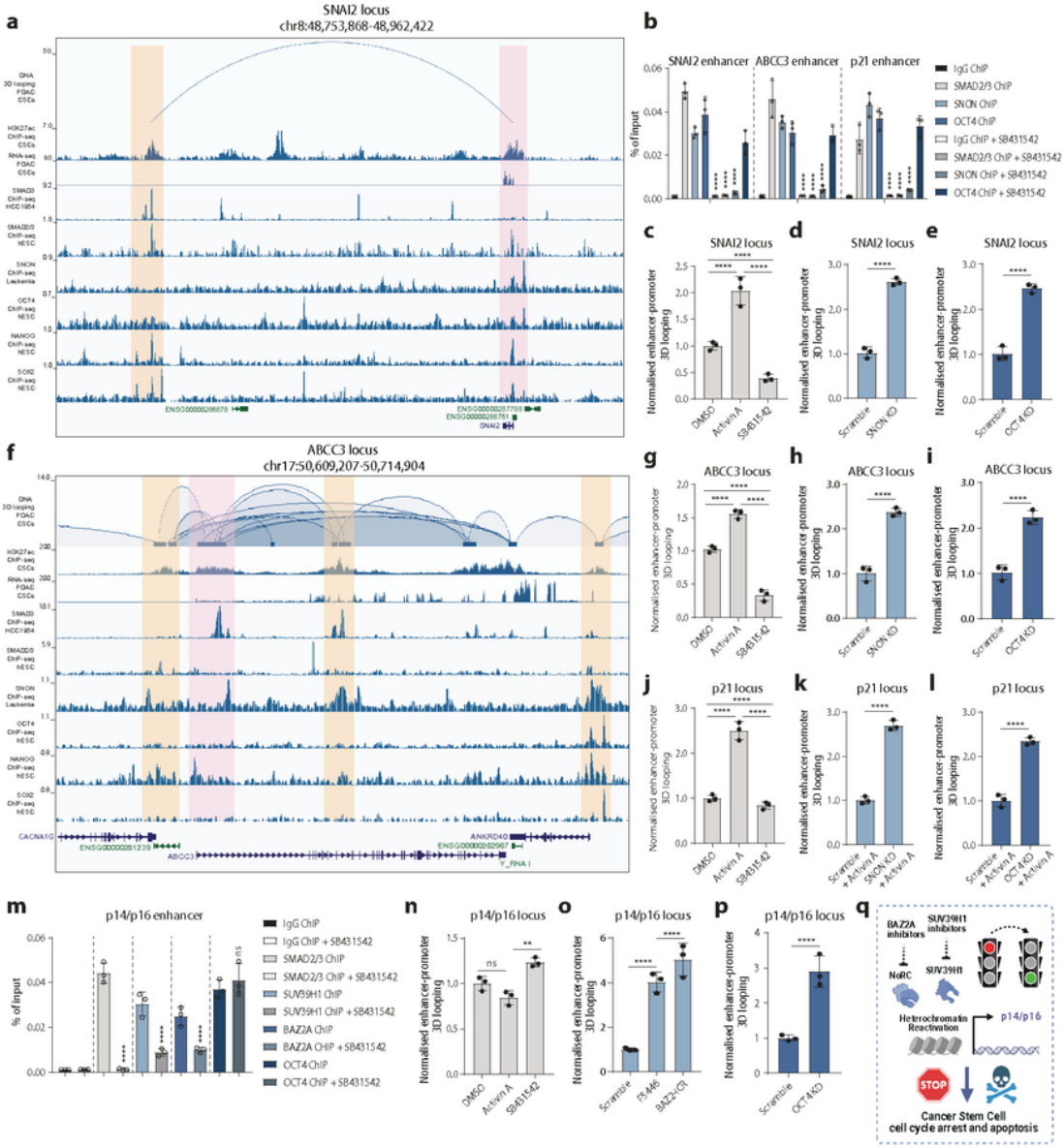

Figure 7

SMAD2/3-OCT4-BAZ2A-SUV39H1 and SMAD2/3-OCT4-SNON complexes regulate enhancer-promoter connectome of CDKI, EMT and chemoresistance loci in CSCs. (**A**) The genomic locus of SNAI2 shows H3K27ac abundance and gene transcription together with 3D chromatin interactions identified by H3K27ac ChIA-PET experiments in CSCs. SMAD2/3, SNON, OCT4, NANOG, SOX2 genomic tracks show their bind to anchor regions. Promoter anchor region is marked with red and the enhancer anchor region

is marked with yellow. (**B**) SMAD2/3 and SNON bind to the 3D chromatin looping anchors at enhancer of SNAI2 (EMT), ABCC3 (chemoresistance) and p21 (cell cycle) locus in a TGFβ/Activin signalling dependent manner whereas OCT4 binds to the anchor without being affected by TGFβ/Activin signalling inhibition in CSCs. (**C-E**) 3C-qPCR analysis of 3D enhancer-promoter interactions at SNAI2 locus in CSCs shows that (C) Activin A signalling, (D) SNON KD, and (E) OCT4 KD increases chromatin looping. (**G-I**) 3C-qPCR analysis of 3D enhancer-promoter interactions at ABCC3 locus in CSCs shows that (G) Activin A signalling, (H) SNON KD, and (I) OCT4 KD increases chromatin looping. (**J-L**) 3C-qPCR analysis of 3D enhancer-promoter interactions at ABCC3 locus in CSCs shows that (G) Activin A signalling, (H) SNON KD, and (I) OCT4 KD increases chromatin looping. (**M**) SMAD2/3, BAZ2A and SUV39H1 bind to the 3D chromatin looping anchors at enhancer of p14/p16 locus in an TGFβ/Activin signalling dependent manner whereas OCT4 binds to the anchor without being affected by TGFβ/Activin signalling inhibition in CSCs. (**N-P**) 3C-qPCR analysis of 3D enhancer-promoter interactions at p14/p16 locus in CSCs shows that (N) Activin A signalling, (O) F5446 and BAZ2A-ICR, and (P) OCT4 KD increases chromatin looping. (**Q**) Schematic depiction of the inhibition of BAZ2A and SUV39H1 that inhibits p14/p16 loci. Statistical analysis was performed by 2-way ANOVA with multiple comparisons with Tukey correction and **** marks adjusted P-value <0.0001, *** is adjusted P-value <0.001, ** is adjusted P-value <0.01, * is adjusted P-value <0.05.

Supplementary Files

This is a list of supplementary files associated with this preprint. Click to download.

- SupplementaryFigures.pdf
- SupplementaryFile.pdf
- SupplementaryInformation.docx
- GraphicalAbstract.pdf